IRS-ASSISTED RAYLEIGH FADING MISO SYSTEMS: BEAMFORMING AND ASYMPTOTIC ANALYSIS

by

Bayan Alnahhas

B.Sc. Hons., Effat University, 2018

A THESIS SUBMITTED IN PARTIAL FULFILLMENT OF

THE REQUIREMENTS FOR THE DEGREE OF

MASTER OF APPLIED SCIENCE

in

The College of Graduate Studies

(Electrical Engineering)

THE UNIVERSITY OF BRITISH COLUMBIA

(Okanagan)

March 2020

The following individuals certify that they have read, and recommend to the College of Graduate Studies for acceptance, a thesis/dissertation entitled:

IRS-ASSISTED RAYLEIGH FADING MISO SYSTEMS: BEAMFORMING AND ASYMPTOTIC ANALYSIS

submitted by Bayan Alnahhas in partial fulfilment of the requirements of the degree of Master of Applied Science

Prof. Anas Chaaban, School of Engineering

Supervisor

Prof. Md. Jahangir Hossain, School of Engineering

Supervisory Committee Member

Prof. Chen Feng, School of Engineering

Supervisory Committee Member

Prof. Mahmudur Fatmi, School of Engineering

University Examiner

Abstract

The recent concept of intelligent reflecting surfaces (IRS) enabled wireless communication can overcome the adverse effects of the wireless channel by manipulating the propagation of the radio waves in the environment. This emerging technology, which relies on low-cost passive reflecting elements, is shown to yield promising performance results in recent studies that often focus on Rayleigh fading environments and assume the availability of perfect channel state information (CSI) at the base station (BS) and the IRS. This work considers the practical setting where only imperfect CSI is available at the BS and the IRS, and studies the downlink sum-rate performance of a multi-user IRS-assisted multiple-input single-output (MISO) system in the asymptotic regime where the number of BS antennas, IRS elements and users grow large. We first derive the MMSE estimates of the IRS-assisted and direct channels under a protocol that ensures that the IRS element stay passive. Then we formulate the signal-to-interference-plus-noise ratio (SINR) and sum rate expressions under maximum ratio transmission (MRT) precoding, and obtain their asymptotically tight deterministic approximations using tools from random matrix theory. The asymptotic performance limits are also derived that reveal that in Rayleigh fading environments, IRS only yields an array gain and loses on the reflect beamforming gain promised by existing works. Simulation results show the tightness of the asymptotic expressions for moderate system dimensions and reveal important insights into how beneficial the IRSs are when the environment has rich scattering as represented in Rayleigh fading. It turns out that IRS introduces high sum-rate gains in noise-limited scenarios whereas the gains start to diminish in interference-limited scenarios.

Lay Summary

With the inevitable increase of interconnected devices and wireless communication demands, it becomes important to consider a new platform for data transmission. The current deployed multi-user systems help accommodate our daily demands of data rates and day-to-day mobile application use. Nevertheless, the future requirements are expected to exponentially increase. Consequently, there is a strong need to improve our current networks to help realize the future vision of data driven society. Intelligent reflecting surface (IRS) comes as an effective and highly potential solution to envision a radically new platform of communication. In an IRS-assisted communication, the environment becomes a controllable factor which IRS can manipulate in favor of user reception by altering the reflection signals in direction of intended users. Such technology is seen as a promising step towards realizing a smart radio environment that optimizes the quality of service for users and achieves high data rate limits in cellular networks.

Preface

This thesis is based on research work conducted under the supervision of Prof. Anas Chaaban and Qurrat-UI-Ain Nadeem (Annie), who is a Post Doctoral Fellow with Prof. Anas Chaaban. The contents of this work along with the numerical results were proofread and validated by Prof. Chaaban and Annie.

Table of Contents

List of Tables

List of Figures

Acknowledgements

I would like to thank Prof. Anas Chaaban for his guidance and support throughout this work. His continuous follow up on work progress and thorough feedback on results were great assets in directing this work. I would also like to thank him for granting me the freedom in my studies and providing me with strong academic flavor in various research directions. I extend my sincere thanks to Annie who closely supervised this work and validated the results. Annie has been an exceptional source of advice and support amid this work and I would sure attribute a lot of the success to her and her diligent help.

My thanks also goes to my colleagues and friends who were an additional fortunate source of support and advice throughout the journey. Finally, deepest thanks to my parents and family who have always and remain a major advocate for my academic journey and an endless source of love and support.

Chapter 1

Introduction

1.1 Background and Motivation

The amount of wireless data communication has been increasing in an exponential pace over the past decades. The significant number of connected devices, the fulfilled demands for real-time video streaming and cell coverage, and the achieved high data rates for advanced mobile applications have become some of the main features that characterize our current wireless networks [BHS17]. Over the past years we have witnessed a major explosion of wireless connectivity and streaming media revolution, where audio and video are delivered on demand over the internet everywhere around the globe. From smart appliances, to smart businesses, traffic systems and industries, our current wireless network, such as the Long Term Evolution (LTE) based cellular wide area networks and satellite services, paved the way to revolutionizing our communication experience. Nevertheless, future demands are always increasing and wireless networks are envisioned to connect a yet greater number of terminals as well as to provide a new competitive data rate limits with ubiquitous cell coverage. In fact, according to Cisco [BDRDR+19], the overall data traffic is expected to increase to 77 exabytes per month by 2022 with number of interconnected devices reaching up to 28.5 billion. As a result, wireless networks seem to consistently move towards a higher need of bandwidth to satisfy the emerging vision of interconnected wireless networks. This exponential trend motivated researchers to find potential solutions that address some fundamental wireless network limitations.

Two timeless facts are evident in wireless networks , demands on wireless throughput will always grow, and the available electromagnetic spectrum will never increase. The performance of wireless networks is typically limited at its physical layer, that is the number of bits transferred between two points depends on the spectrum availability, laws of electromagnetic propagation and principles of information theory [Mar15, RPL+13, Ngo15]. As shown in Fig. 1.1, a typical cellular

network consists of a number of cells, where in each cell, a base station equipped with M antennas serves K number of user terminals. To improve the wireless communication performance, research typically approaches network problem through three basic solution directions: (i) deploying more access points per cell (known as cell densification), (ii) using more spectral bands, or (iii) increasing spectral efficiency, that is the number of bits that are conveyed in a given resource block or unit bandwidth [MLYN16]. While the stringent expectations of emerging wireless networks are likely to require an ever-increasing use of bandwidth to realize the future vision of internet of things (IoT) and emerging wireless networks such as 5G and beyond, numerous leading research work help develop solutions that make an efficient use of the available spectrum band while at the same time provide a reliable wireless throughput throughout a designated area [KUV19, BSW$^+$19, AH16].

In the light of this, we will take a step back and introduce a revolutionary technology, known as multiple input and multiple output (MIMO), where a BS is equipped with large number of antennas serves many users in the same time-frequency resource block [Ngo15, GKH$^+$07]. The technology had significantly changed the vision of wireless networks for decades and paved the way to realizing our current deployed network infrastructure. In the following subsections, we will provide a brief background on the MIMO technology and how it works. We will then follow this with important techniques utilized, such as beamforming, which helps leverage the additional spatial dimensions provided in MIMO systems by directing a beam to intended user and thus improving user's signal reception. Finally, we'll introduce random matrix theory (RMT) that is used to study the asymptotic performance of the system and help us realize the benefits of large system dimensions in solving important optimization problems.

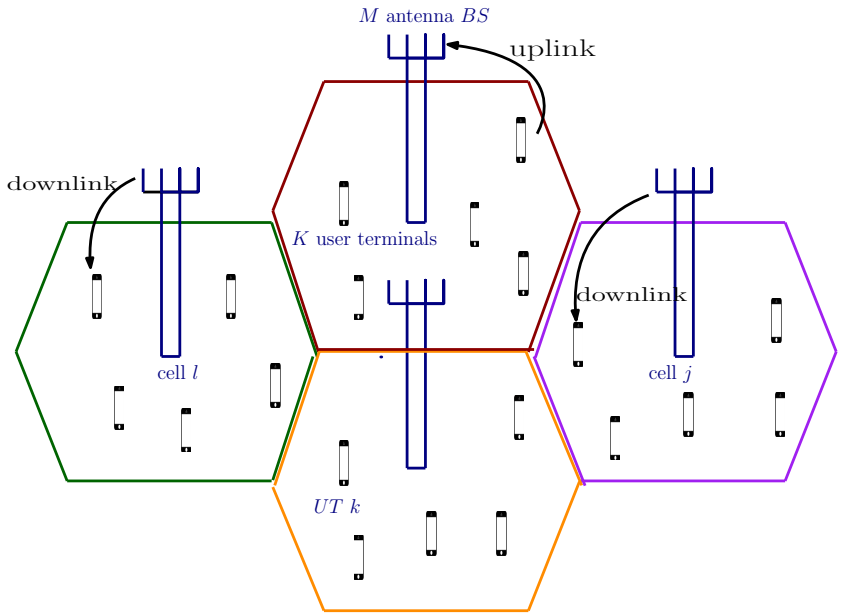

Figure 1.1: Multiuser cellular network

1.1.1 MIMO Systems

Multiple input multiple output (MIMO) technology has caught major attention over the past decades and was seen as a viable approach to substantial improvement in spectral efficiency. The evolutionary technology is known to enhance the reliability of communication by providing substantial multiplexing and diversity gains. In wireless communication, the transmitted signal suffers from fading due to multipath propagation and shadowing due to large obstacles between the transmitter and receiver. By deploying multiple antennas at the BS and/or receiver, multiple streams can be sent over the channel, and thus data may be spatially multiplexed onto a MIMO channel providing an R-fold capacity increase, where R is the number of independent channels determined by the rank of the channel matrix [TV05, Gol05]. MIMO technology is now relatively mature and is incorporated in the wireless broadband standards such as LTE-Advanced to support our current demand of bandwidth [JKL+17]. In this subsection, we will highlight the evolution of MIMO technology while discussing the performance at each stage.

MIMO systems are mainly categorized into three categories, namely point to point MIMO, Multiuser MIMO and Massive MIMO [MLYN16]. We will provide a brief outline for every classi-

fication, as the process of evolving from one classification to another will pave the way to a stronger understanding on the main work of this dissertation, i.e. IRS-assisted MIMO systems [BSW+19].

A point-to-point MIMO link consists of a BS equipped with a concentrated array of M antennas communicating with a user equipped with concentrated array of K antennas. The fundamental idea of point to point systems is that in every channel use, the BS transmits a signal vector, and the user receives a signal vector that is a linear combination of transmitted signal and the combining coefficients of the channel matrix, which are determined by the channel propagation [Gol05]. By Shannon's theorem, the uplink and downlink capacity in bits/s/Hz of a MIMO point-to-point systems with Gaussian noise can be defined as:

$$\mathbf{C} = \max_{\mathbf{D}_v} \quad \log_2 |\mathbf{I}_K + \rho \mathbf{G}\mathbf{D}_v\mathbf{G}^H| \tag{1.1a}$$

$$\text{s.t.} \quad tr(\mathbf{D}_v) \leq 1, \tag{1.1b}$$

where the optimization is over the positive semi-definite covariance matrix $\mathbf{D}_v \in \mathbb{C}^{M\times M}$, and $\mathbf{G}$ is an $K \times M$ channel gain of the channel matrix between the BS and K user terminals, $\mathbf{I}_K$ is a $K \times K$ identity matrix, the superscript H denotes to the conjugate transpose, and ρ is the signal to noise ratio (SNR) which is proportional to the corresponding total radiated powers. Using singular value decomposition (SVD), we can rewrite the channel matrix as $\mathbf{G} = \mathbf{U}\mathbf{A}\mathbf{V}^H$, where $\mathbf{U}$ is an $K \times K$ unitary matrix, $\mathbf{V}$ is an $M \times M$ unitary matrix and $\mathbf{A}$ is $K \times M$ diagonal matrix with non-negative entries. The diagonal elements σ_i of matrix $\mathbf{A}$ are the singular values of channel matrix $\mathbf{G}$, where $\mathbf{G}$ is of rank R with R positive singular values, satisfying $R \leq \min(M, K)$. The SVD allows us to convert the MIMO system into parallel, non interfering channels by pre-multipying the input with matrix $\mathbf{V}$ (i.e transmit precoding) and post-multiplying the output by the matrix $\mathbf{U}^H$ [BCC+07]. The result is R parallel non-interfering channels, also known as eigenmodes of the channel. Using waterfilling algorithm, we can optimally allocate powers over the parallel channels, such that:

$$P_i = (\mu - \frac{1}{\rho\sigma_i^2})^+, 1 \leq i \leq R \tag{1.2}$$

where P_i is the power associated with the i'th transmitted symbol, $(\cdot)^+$ defines max(·,0), and μ is the water level chosen such that $\sum_{i=1}^{R} P_i = 1$. The optimal covariance matrix, (i.e $\mathbf{D}_v$ that achieves the maximum in (1.1)) is $\mathbf{D}_v = \mathbf{VPV}^H$, where $\mathbf{P} = diag(P_1, \ldots, P_R, 0, \ldots, 0) \in \mathbb{C}^{M \times M}$. A more detailed explanation on SVD and waterfilling algorithm can be found in [TV05, BCC+07].

Notice that under certain channel assumptions, such as sufficiently large value of signal to noise ratio (SNR) and a rich scattering environment modeled by independent Rayleigh fading, where the channel matrix $\mathbf{G}$ becomes of full rank, such that $R = \min(M, K)$, and under the use of asymptotic random matrix theory, $\mathbf{C}$ in (1.1) scales linearly with min(M,K) and logarithmically with SNR [MLYN16, NLM13]. This can be approximately expressed as:

$$\mathbf{C} \propto \min(M, K) \log_2(\rho), \tag{1.3}$$

where M and K are the antenna array size of BS and receiver, respectively. Therefore, the spectral efficiency can be simultaneously increased by deploying large arrays in the transmitter and receiver, making M and K large.

Nevertheless, in practice, point to point MIMO systems fall back in several factors. First, the equipment is complicated and requires independent RF chains per antenna as well as the use of advanced digital signal processing to separate the data streams. Second, scaling up the number of antennas requires a proportional amount of training time (time required for the receiver to learn the channel matrix). Third, to realize the benefits in equation shown in (1.3), the propagation channel must support at least min (M,K) independent channels. This is not typically the case in propagation environments, as line of sight (LOS) condition presents a particular challenge for compact arrays, wherein the channel matrix would have a minimum rank of one thus permitting only one data stream [Mar15, RPL+13].

Multiuser (MU) MIMO system help mitigate some drawbacks of point-to-point MIMO system. MU-MIMO is essentially equivalent to starting with a MIMO point to point link, and breaking the single K antenna user terminal to K autonomous single antenna users [LLS+14]. The illustration shown in Fig.1.2 shows a conventional MU-MIMO system, where a BS equipped with M antennas communicates with K single antenna users. It is worth noting that though the K users do not

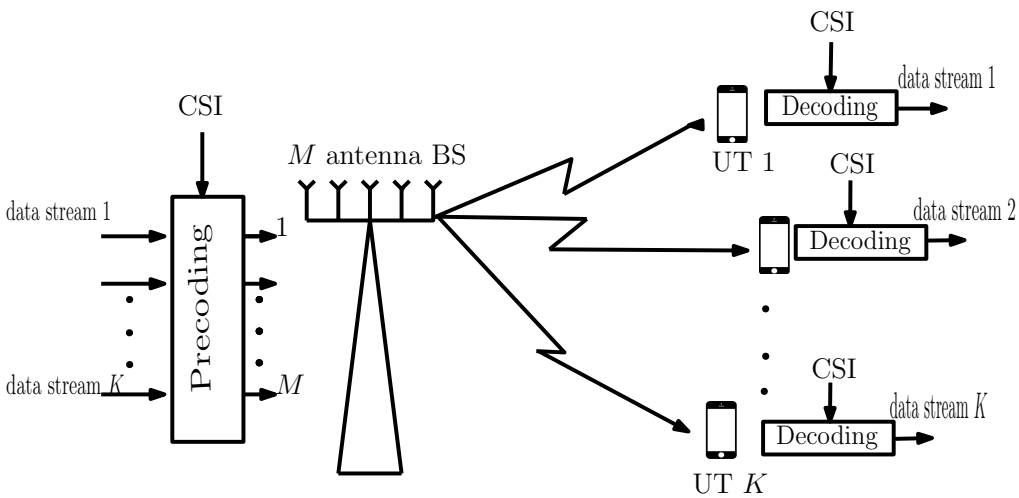

Figure 1.2: Multiuser MIMO system setup

cooperate in a mutiuser system, this does not compromise on the overall capacity or sum throughput of the system. The Shannon's sum capacity in the uplink and downlink links can be expressed as follows [VT03]:

$$\mathbf{C}^{ul} = \log_2 |\mathbf{I}_M + \rho_{ul}\mathbf{G}\mathbf{G}^H|, \tag{1.4}$$

$$\mathbf{C}^{dl} = \max_{v_m \geq 0} \quad \log_2 |\mathbf{I}_M + \rho_{dl}\mathbf{G}^H\mathbf{D}_v\mathbf{G}| \tag{1.5a}$$

$$\text{s.t.} \quad \sum_{m=1}^{M} v_m \leq 1, \quad \forall m, \tag{1.5b}$$

where $\mathbf{D}_v$ is a diagonal covariance matrix with diagonal elements $\mathbf{v} = [v_1 \ldots v_M]$, $\mathbf{G}$ is an $M \times K$ channel matrix, and ρ_{dl}/ρ_{ul} is the downlink/uplink SNR. According to the problem formulated in (1.5), the downlink capacity for MU MIMO requires a solution of a convex optimization problem.

MU-MIMO systems possess two major practical limitations. Achieving the capacity expressed in (1.5) requires a complicated coding technique known as dirty paper coding, whose complexity grows exponentially with the system dimension at both the BS and user ends. Additionally, in the downlink, the BS and user terminals must both know the channel matrix $\mathbf{G}$, which requires

considerable amount of resource for pilot transmission. Nevertheless, MU-MIMO systems hold two important advantages over point to-point MIMO systems, that is MU-MIMO systems are less sensitive to assumptions on the propagation environment, and do not require multiple antennas at the user end [Mar15, GKH+07].

To address the scalability issue that MU-MIMO faces, Massive MIMO comes as a potential solution and is considered as a salable version of MU-MIMO. Massive MIMO systems breaks the scalability barrier by using simple linear precoders while at the same time achieving a better performance than a non-Massive MIMO system [Mar15]. Each BS in a Massive MIMO systems is equipped with large number of M antennas serving large number of K users. Under time division duplexing (TDD) operation, only the BS is required to learn the channel matrix $\mathbf{G}$, where the time required to obtain the CSI is independent of BS antenna array size. Furthermore, as number of BS antennas increases, the propagation environment becomes favorable [TV05], i.e channels become mutually orthogonal, therefore simple linear precoding/decoding techniques are found optimal and the system's performance approaches Shannon's limit.

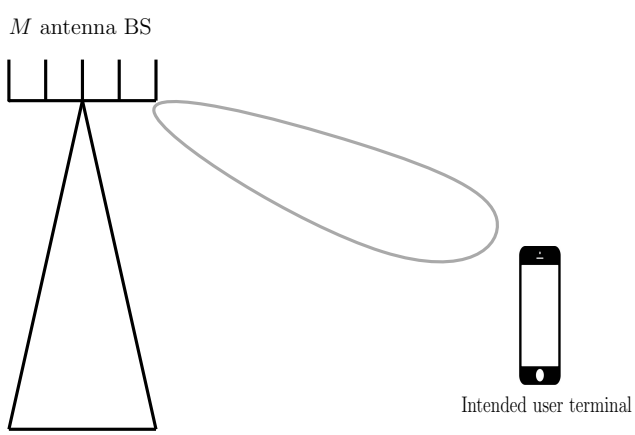

Figure 1.3: Beamforming representation

Increasing the antenna array size has several advantageous factors that are worth noting. In the downlink, the BS ensures that each user terminal receives only the signal intended for it. This is accomplished by creating a beam with a narrow angular window centered in the direction of the terminal. Larger the number of BS antennas are, the narrower the radiated beam is. By properly

choosing the transmitted waveforms, signals' scattering and reflecting components will experience constructive superposition at the intended terminal and destructive superposition at the non-intended terminals [TV05]. We refer to this technique used to produce directed beams as "beamforming", as depicted in Fig.1.3. The more antennas deployed at the BS, the more sharply focused the beam power is at the intended end. Another important consequence of deploying large number of antennas is phenomenon known as channel hardening. The significance of channel hardening lies in the fact that small scale fading effects tend to disappear as M grows large [WCDS12a]. To clarify this point, consider an M dimensional channel response vector $\mathbf{h}$ and beamforming vector $\mathbf{a}$. As M grows large, and by the law of large numbers, the scalar channel gain $\mathbf{h}^T\mathbf{a}$ becomes close to its expected value, i.e. $\mathbb{E}[\mathbf{h}^T\mathbf{a}]$, which is a deterministic value. The resulting scalar effective channel facilitates the use of simple schemes for resource allocation and power control. This holds great advantage with regards to solving optimization problems, as we'll see later in this thesis. Section 1.1.4 in this chapter will further elaborate on the benefits of studying the systems in an asymptotic regime and the benefit of using random matrix theory (RMT) in system analysis.

1.1.2 FDD/TDD Systems and Channel Estimation

In this section, we will highlight two known duplexing modes which MIMO systems operate in, namely Frequency Division Duplexing (FDD) and Time Division Duplexing (TDD) modes. In a practical system, the BS does not know the exact channel state information (CSI) and has to estimate it instead. Depending on the duplexing mode, the channel estimation schemes differ. We will briefly discuss how is the channel estimation run in each mode and follow this to introduce a reliable channel estimation technique known as linear minimum mean square error (LMMSE) estimation.

- Time Division Duplexing (TDD) operation: In the TDD mode, the uplink and downlink transmission use the same frequency spectrum, but different time slots. In addition, the uplink and downlink channels are reciprocal. The BS learns the uplink channel from uplink pilots and uses it as a legitimate estimate for the downlink channel. More precisely, the process is as follows: during the uplink transmission, K users transmit K orthogonal pilots to the BS. The BS estimates the uplink channel based on the received pilots and uses it to detect

the signals transmitted. During the downlink transmission, the BS uses the channel estimated in the uplink to precode the transmit symbols. The users will also need to know the effective channel gain to detect their signals, therefore the BS sends K beamformed pilots and each user can estimate the effective channel gain based on the received pilot [TV05, Gol05, Ngo15].

- Frequency Division Duplexing (FDD) operation: In the FDD mode, the uplink and downlink channels lack reciprocity. The uplink and downlink channels uses different frequency spectrum. To obtain the CSI in the downlink transmission, the BS transmits M orthogonal pilots to K users, where each user estimates the channel and feeds it back to the BS through the uplink. Similarly, in the uplink transmission, K users transmit K orthogonal pilots sequences to the BS for channel estimation purpose [TV05, Ngo15].

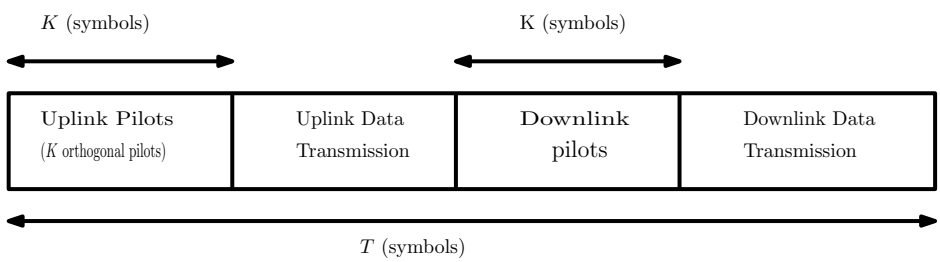

Figure 1.4: Channel estimation in TDD system

It is important note that sending pilots consumes resources. Specifically speaking, during the time-frequency period in which the channel is static (known as the coherence period), each transmitting antenna needs to be assigned a unique pilot waveform and they need to be orthogonal. In other words, if K antennas transmit K orthogonal pilots in uplink, at least K slots in the coherence period have to be designated for pilot transmission, thus resource consuming [Mar06]. The symbol slot structure shown in Fig. 1.4 illustrates the training process where it is assumed that the channel stays constant over T symbols and $K < T$. In this illustration, at least K symbols are needed as uplink pilots and K symbols for downlink beamformed pilots, thus at least $2K$ symbols from T symbols are dedicated for training process. With the continuous increase in number of wirelessly connected users, it is worth considering the resources used in different MIMO system settings. Table 1.1 summarizes the amount of resources needed for pilots and CSI feedback for each Point-to-point MIMO, MU MIMO and Massive MIMO operating in both the TDD and FDD schemes.

To explain the resource use shown in the table, let's look at the conventional multi-user MIMO as an example, and compare the TDD and FDD mode resource usage. Recall that in FDD mode, the BS learns the downlink channel by communicating M pilots to user terminals, which estimate the downlink channel and communicate the estimated CSI coefficients back to BS in the uplink. The BS also learns the uplink channel by listening to K pilots sent by user terminal via the uplink. This sums up to K pilots and M CSI coefficients resource usage in the uplink and M pilots in the downlink. Now since the TDD mode leverages reciprocity advantage, the BS can learn the uplink channel by listening to the K pilots sent by terminals in the uplink and use it a legitimate estimate for downlink channel. The user terminal also requires the knowledge of effective channel gain for decoding, thus M pilots are required for the downlink. This indeed sums up for K pilots in the uplink and M pilots in the downlink. A similar scenario occurs in Massive MIMO under FDD mode with same resource usage, but we can notice that in TDD mode the large system dimension advantage kicks in, and due to the favorable condition, no pilots are required in the downlink.

	FDD		TDD	
	Uplink	Downlink	Uplink	Downlink
Point-to-point ($M \times K$) MIMO	K pilots	M pilots	K pilots	M pilots
Conventional Multiusers MIMO	K pilots+ M CSI-coeff.	M pilots	K pilots	M pilots
Massive MIMO	K pilots+ M CSI-coeff.	M pilots	K pilots	none

Table 1.1: The minimum number of samples consumed for pilot transmission and CSI feedback in terms of total number of per coherence interval for three MIMO variants, while assuming $M > K$

Therefore, massive MIMO system operating in TDD stands out, as the number of pilots required is independent of the number of BS antennas, and the CSI feedback is not required. For this reason, Massive MIMO systems are seen as a promising candidate given its unlimited scalability [LETM14, RPL+13].

Channel Estimation

The performance of wireless network heavily depends on the quality of channel estimates. Estimating a random channel is often a complicated process, and the popular Bayesian estimators (MMSE and MAP) are difficult to determine in closed form as well as computationally expensive to implement [Kay97]. For this reason, it is a practical solution to retain the MMSE criterion but constrain the estimator to be linear. In this subsection, we will introduce the linear minimum mean square estimation (LMMSE) criterion. To begin, let's consider a conventional and simplified MU-MIMO system, wherein an M-antenna BS is communicating with K single antenna users and operating in a TDD scheme. In such a topology, the received signal at user k can be expressed as follows:

$$y_k = \mathbf{h}_k^H \mathbf{x} + n_k, \tag{1.6}$$

where $\mathbf{h}_k \sim \mathcal{CN}(\mathbf{0}, \beta_k \mathbf{I}_M) \in \mathbb{C}^{M\times 1}$ is the channel between user k and BS modeled as an i.i.d. Rayleigh fading channel with pathloss parameter β_k, $\mathbf{x} \in \mathbb{C}^{M\times 1}$ is the data signal vector, and $n_k \sim \mathcal{CN}(0, \sigma^2)$ [MSI17, WCDS12a].

During the training phase, users transmit K mutually orthogonal pilot sequences to BS in the uplink. The BS essentially aims at estimating $\mathbf{h}_k$ from the observed signal by first correlating it with the pilot sequence to obtain a training signal, which it uses to calculate the channel estimate. The training signal can be expressed as follows:

$$\mathbf{y}_k^{tr} = \mathbf{h}_k + \mathbf{n}_k^{UL}, \quad k = 1 \ldots K, \tag{1.7}$$

where $\mathbf{n}_k^{UL} \sim \mathcal{CN}(\mathbf{0}, \frac{1}{\rho_{tr}}\mathbf{I}_M)$ and ρ_{tr} is the training SINR. The channel estimate $\hat{\mathbf{h}}_k$ can be computed from $\mathbf{y}_k^{tr}$ such that, $\hat{\mathbf{h}}_k = \mathbf{A}\mathbf{y}_k^{tr}$ where $\mathbf{A}$ is some transformation weight matrix that operates on the training signal to obtain the channel estimate [MJ19a]. Therefore, the BS aims at finding the optimal weighting coefficients that minimizes $\mathbb{E}[|\hat{\mathbf{h}}_k - \mathbf{h}_k|^2]$= $\mathbb{E}[|\mathbf{A}\mathbf{y}_k^{tr} - \mathbf{h}_k|^2]$ to the following:

$$\hat{\mathbf{h}}_k = \mathbb{E}[\mathbf{y}_k^{tr}\mathbf{h}_k^H](\mathbb{E}[\mathbf{h}_k^{tr}\mathbf{h}_k^{trH}])^{-1}\mathbf{y}_k^{tr}, \tag{1.8}$$

where $\mathbb{E}[\mathbf{h}_k^{tr}\mathbf{h}_k^{trH}]$ is the covariance matrix of $\mathbf{h}_k$ and $\mathbb{E}[\mathbf{y}_k^{tr}\mathbf{h}_k^H]$ is a cross-covariance matrix [Kay97]. When estimating a Gaussian vector, i.e. $\mathbf{h}_k$ in our example, the MMSE estimator becomes linear.

Therefore, to find the MMSE estimator for a Gaussian vector, it is sufficient to find the LMMSE estimator. Notice that MMSE estimate in (1.8) requires the second order statistical properties of the data in a random process, therefore it is considered as a reliable and practical estimation approach for all realizations in a random process.

1.1.3 Precoding Techniques

Complex signal processing techniques such as maximum likelihood detection are required to provide an optimal performance for wireless system signal detection performance. Nevertheless, it has been shown in [RPL+13, Mar10], that for a BS with large number of antennas, linear processing schemes are found nearly optimal. This significantly reduces the computational complexity, which adds another advantage for massive MIMO systems. In this subsection, we'll introduce some main linear precoding techniques used in MIMO systems.

We will consider a similar setup as that introduced in the previous section, where a BS with M antennas is communicating with K single antenna users while using linear precoders. The signal transmitted from M-antenna BS, $\mathbf{x}$ is a linear combination of symbols intended for K users. The linearly precoded signal can be defined as:

$$\mathbf{x} = \sqrt{\alpha}\mathbf{W}\mathbf{s}, \tag{1.9}$$

where $\mathbf{s} \in \mathbb{C}^{K\times 1}$ is the transmitted source information before precoding, $\mathbf{W} \in \mathbb{C}^{M\times K}$ is the linear precoding matrix, and $\alpha = \frac{1}{tr(\mathbf{W}\mathbf{W}^H)}$ is the normalization constant to satisfy the power constraint $\mathbb{E}[||\mathbf{x}||^2] = 1$.

In TDD mode, the downlink signal received at the k'th user terminal can be expressed as follows:

$$y_k^{dl} = \sqrt{\alpha\rho_{dl}}\mathbf{h}_k^T\mathbf{W}\mathbf{s} + n_k, \tag{1.10}$$

$$= \sqrt{\alpha\rho_{dl}}\mathbf{h}_k^T\mathbf{w}_k s_k + \sqrt{\alpha\rho_{dl}}\sum_{l\neq k}\mathbf{h}_k^T\mathbf{w}_l s_l + n_k, \tag{1.11}$$

where $n_k \sim \mathcal{CN}(0, \sigma^2)$ is the Gaussian noise, $\mathbf{h}_k \in \mathbb{C}^{M\times 1}$ and ρ_{dl} is the downlink SINR.

Therefore the SINR at the k'th user can be expressed as follows:

$$SINR_k = \frac{\alpha\rho_{dl}|\mathbf{h}_k^T\mathbf{w}_k|^2}{\alpha\rho_{dl}\sum_{l\neq k}|\mathbf{h}_k^T\mathbf{w}_l|^2 + \sigma^2}. \tag{1.12}$$

Maximum Ratio Transmission

Maximum Ration Transmission (MRT) also known as Matched Filter (MF) is simply the conjugate of the downlink channel, i.e:

$$\mathbf{W}_{MRT} = \mathbf{H}^*, \tag{1.13}$$

where $\mathbf{H} = [\mathbf{h}_1, \ldots, \mathbf{h}_K] \in \mathbb{C}^{M\times K}$,$\mathbf{h}_k \in \mathbb{C}^{M\times 1}$, and $\mathbf{H}^* = [\mathbf{h}_1^*, \ldots, \mathbf{h}_K^*] \in \mathbb{C}^{M\times K}$.

Therefore the received signal at user k can be expressed as:

$$y_k^{dl} = \sqrt{\alpha\rho_{dl}}\mathbf{h}_k^T\mathbf{H}^*\mathbf{s} + n_k, \tag{1.14}$$

The MRT precoder is known to maximize the signal gain at the intended end, but, as shown in [BSHD15], for close values of M and K, the performance of massive MIMO degenerates due to the strong inter-user interference. When increasing the number of BS antennas, the channel vectors in $\mathbf{H}$ become close to mutually orthogonal and thus the term $\mathbf{H}^T\mathbf{H}^*$ approaches a diagonal matrix. This asymptotic property cancels out the inter-user interference and makes the MRT precoder an optimal solution [FHX+18]. We will be using this technique in our proposed system model in this work.

Zero-Forcing

Zero-forcing (ZF) precoding is a precoding technique that aims at eliminating the interference at the expense of channel capacity. This precoder eliminates the interference by transmitting the signal towards the intended user while nulling in direction of other users. The Zero-forcing precoder obtained is expressed as follows:

$$\mathbf{W}_{ZF} = \mathbf{H}^*(\mathbf{H}^T\mathbf{H}^*)^{-1}. \tag{1.15}$$

Therefore the corresponding received signal is defined as follows:

$$y_k^{dl} = \sqrt{\alpha\rho_{dl}}\mathbf{h}_k^T\mathbf{H}^*(\mathbf{H}^T\mathbf{H}^*)^{-1}\mathbf{s} + n_k. \tag{1.16}$$

This technique is optimal in the absence of noise, but in the presence of noise, it amplifies the noise power.

Regularized Zero Forcing

The Regularized Zero Forcing (RZF) is a precoding technique that holds popularity in its ability in trading off the advantages of MF and ZF precoders. According to [FHX+18, BSHD15], the RZF precoder can be defined as follows:

$$\mathbf{W}_{RZF} = \mathbf{H}^*(\mathbf{H}^T\mathbf{H}^* + \mathbf{X} + \lambda\mathbf{I}_K)^{-1}. \tag{1.17}$$

The above definition of an RZF precoder can be seen as a ZF precoder regularized by an Hermitian non-negative matrix $\mathbf{X}$ and regularization factor λ.

The received signal can thus be defined as follows:

$$y_k^{dl} = \sqrt{\alpha\rho_{dl}}\mathbf{h}_k^T\mathbf{H}^*(\mathbf{H}^T\mathbf{H}^* + \mathbf{X} + \lambda\mathbf{I}_K)^{-1}\mathbf{s} + n_k. \tag{1.18}$$

Notice that the choice of $\mathbf{X}$ and λ affect the property of RZF precoder. Specifically, if $\mathbf{X} = 0$ then (1.17) becomes an MF precoder when $\lambda \to \infty$, while an ZF precoder when $\lambda \to 0$. The design of these parameters typically depends on the system's optimization scheme and design [FHX+18, Ngo15].

1.1.4 Asymptotic Analysis and Random Matrix Theory

In this section we will highlight the significance of studying the wireless system in an asymptotic regime, an approach that is considered in this thesis when analyzing the asymptotic performance of an IRS-assisted MIMO system.

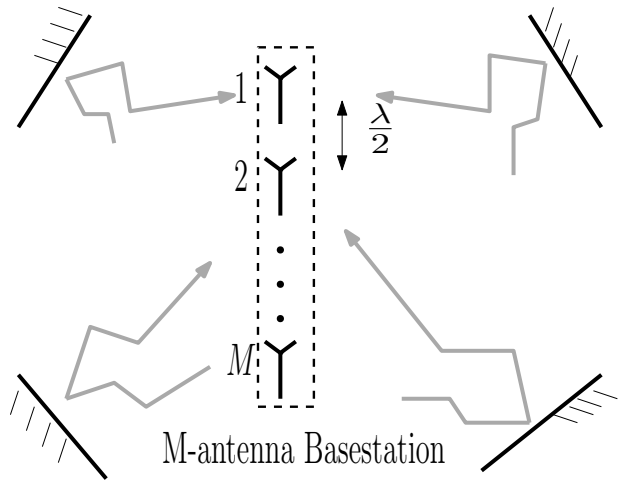

Figure 1.5: Isotropic scattering, approximated as a rayleigh fading

Let us consider a setting where a massive MIMO system is deployed in a single cell and operates in an isotropic scattering environment, i.e. channels are modeled are i.i.d. Rayleigh fading, as depicted in Fig.1.5. The antenna separation is chosen so as to satisfy the spatial correlation function of the wave equation $r(d) = \text{sinc}(2d/\lambda)$ were d is the spatial separation of the two locations at which the field is sampled [MBB+00, 3Gp10]. The channel distribution, Rayleigh fading, can be justified by the central limit theorem by assuming that each antenna receives a superposition of many waveforms that originates from independent scattering [MLYN16]. Since a wireless fading channel is practically random in nature, system's propagation analysis involves studying the network's performance on average. For an i.i.d. Rayleigh fading model with channel matrix $\mathbf{H} = [\mathbf{h}_1, \ldots, \mathbf{h}_K] \in \mathbb{C}^{M\times K}$, $\mathbb{E}[|h_k^m|^2] = \beta_k$, and $\mathbb{E}[h_k^{m*} h_l^m] = 0$ for $l \neq k$, where h_k^m is the m'th element in channel vector $\mathbf{h}_k$, then by the law of large numbers:

$$\frac{1}{M}||\mathbf{h}_k||^2 \to \beta_k, \quad M \to \infty, \quad k = 1, \ldots, K, \tag{1.19}$$

$$\frac{1}{M}\mathbf{h}_k^H \mathbf{h}_l \to 0, \quad M \to \infty, \quad k \neq l. \tag{1.20}$$

Therefore, asymptotically, an independent Rayleigh fading channel attains a favorable propagation, i.e. the user's channel vectors are almost mutually orthogonal [MLYN16].

Generally speaking, multiple antenna systems heavily rely on signal processing and thus are more concerned with vectorial inputs rather than scalar inputs. Therefore, it is of great research and

system analysis interest to show that a functional of a random matrix $\mathbf{H}$ can be well approximated by a deterministic quantity which only depends on the statistical property of $\mathbf{H}$ [CD11, TV04]. To further elaborate on this point, consider a sequence of K i.i.d. random vectors randomly drawn from an M-variate zero mean random process, such that $\mathbf{x}_1, \mathbf{x}_2 \ldots, \mathbf{x}_K \in \mathbb{C}^{M\times 1}$, where K/M is a fixed ratio, then,

$$\mathbf{R}_K = \frac{1}{K}\sum_{i=1}^{K} \mathbf{x}_i \mathbf{x}_i^H \xrightarrow[K\to\infty]{a.s.} \mathbf{R} \triangleq \mathbb{E}[\mathbf{x}_1 \mathbf{x}_1^H], \tag{1.21}$$

where $a.s.$ stands for almost surely, and $\mathbf{R}_K$ is the empirical covariance matrix computed from observed vector samples. The convergence property holds for any matrix norm, i.e. $||\mathbf{R} - \mathbf{R}_K|| \to 0$ with probability 1. As K is chosen very large for a fixed M (keeping K/M fixed), $\mathbf{R}_K$ is a good approximation of $\mathbf{R}$, and the convergence property holds. These deterministic quantities derived from random matrices are usually given in a concise form as (1.21) shows, and helps draw some insights about important system parameters as well as provide a strong tool to build simple schemes for resource allocation and power control for large dimension MIMO system.

Therefore with the increase of system's dimension, i.e. as the number of antennas grow large, the random matrix theory (RMT) advantage kicks in, and what was random start to behave in deterministic manner [WCDS12b, RPL+13]. This becomes particularly important when formulating the signal to interference noise ratio (SINR) and other system's performance metrics in an asymptotic regime, as we will see in Chapter 3. We will make use of large system dimension to obtain insights on system's behavior. More specifically, using tools from random matrix theory (RMT), we study the asymptotic performance of the IRS-assisted system, where IRS is equipped with N reflecting elements, by deriving the deterministic approximations of the SINR and the sum-rate, which are tight in the limit $M, N, K \to \infty$.

1.2 Intelligent Reflecting Surfaces

The emerging future wireless networks including fifth generation (5G) and beyond are not only anticipated to fulfill the challenging demands of increased connectivity, data reliability and speed,

but also to successfully realize a distributed intelligent communication platform that meets the requirements of the current growing wireless communication direction. The new user requirements, new application and communication trends will bring about challenging problems that motivate researchers to envision a radically different communication platform [YXXL19, Ren19, BRdR+19]. Sixth-G is in fact expected to accommodate a society that is typically data driven, thus enabling autonomous systems with unlimited wireless connectivity and negligible latency [CSAJ19]. Nevertheless, as works on previous wireless generations have shown, the advent of a new generation is usually accompanied with the inevitable high energy consumption and considerable hardware/spectrum deployment cost [BIK+16, WLC+17, MIA16]. Under these concerns and over the past few decades a growing interest in investigating new technological techniques that help meet the challenging demands of emerging wireless networks while at the same time provide an improved spectral and energy consumption has notably been increasing in wireless communication research.

1.2.1 Background and Motivation

Various technological advances, including massive multiple-input multiple-output (MIMO), millimeter wave (mmWave) communication, and network densification, are leading the emergence of 5G networks. Their advantages are indisputable, but they face two main practical limitations. First, they consume a lot of power and incur high hardware/spectrum deployment costs which are critical issues for practical implementation [BIK+16, WLC+17, MIA16], and second, they struggle to provide quality of service guarantee in harsh propagation environments, due to the lack of control over the wireless channel. Wireless research has always focused on the design and optimization the communication end-points and the transmission protocols that can adapt to the time-varying characteristics of the propagation environment. The wireless environment (or channel) itself is generally assumed uncontrollable and often acts as an adversary to the communication process. For example, high path loss especially at mmWave frequencies limits the network coverage and results in blockages, multi-path propagation results in fading, poor scattering results in rank-deficient MIMO channels while anomalous reflections and refractions from environmental objects result in uncontrollable interference.

In light of these limitations, the biggest challenge has been to find a way to control the propaga-

tion of radio waves in the environment in an energy-efficient way to improve the system performance without increasing the power consumption, resulting in green, sustainable and pervasive future wireless networks. A transformative concept that addresses this need is that of a smart propagation environment enabled by intelligent reflecting surfaces (IRSs), also known as reconfigurable intelligent surfaces (RISs) [WZ19c, Ren19], that can be deployed on the environmental objects to customize the propagation of radio waves in the environment through controlled reflections. In the recent literature on this concept, IRS is abstracted as a planar array of large number of passive reflecting elements, where each element can be remotely and independently reconfigured to induce a desired phase shift onto the incident electromagnetic waves. By properly adjusting the phase shifts induced by all passive elements of the IRS, the reflected electromagnetic waves can add constructively at the desired user to achieve high received signal power and add destructively at the non-intended users to mitigate the interference effect.

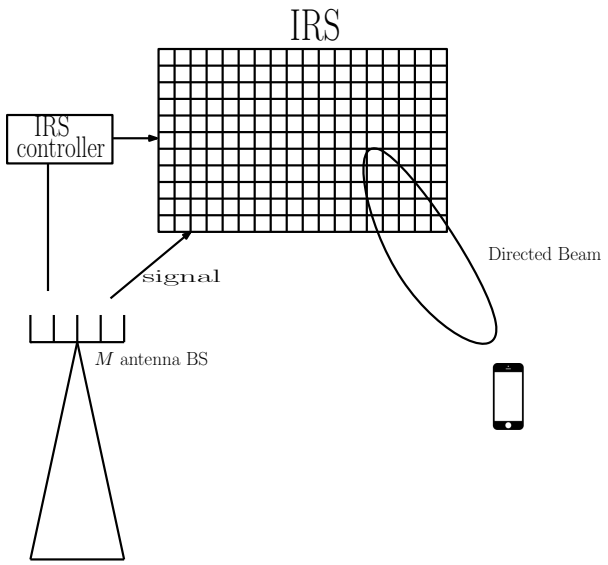

Figure 1.6: IRS-assisted wireless transmission: IRS facilitates beamforming by directing a beam centered at the user end

Current implementations of IRSs include reflect-arrays and reconfigurable meta-surfaces, which can manipulate the incident waves in a passive manner without generating new radio signals and therefore without incurring any notable power consumption. Hence, as Fig. 1.6 shows, an IRS can be seen as array of meta-atoms that each scatter the incoming signal by a controllable phase to produces a directed beam as a product of the joint effect of all induced phase-shifts [ZBM+19].

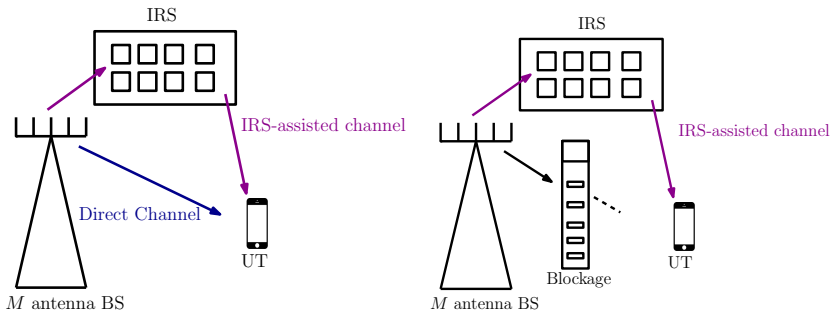

(a) An IRS-assisted system with a direct channel path between the BS and user terminal

(b) An IRS-assisted system with a blockage between the BS and user terminal

Figure 1.7: IRS-assisted system depicting two practical scenarios

To conceptualize the benefit of IRS in MISO systems, let us consider two practical settings as shown in Fig. 1.7. First setting is in which the information signal is transmitted to user via two paths, an IRS-assisted path and a direct BS-user path, as shown in Fig. 1.7(a). The BS typically applies the beamforming technique on the transmitted signal to direct the beam power to the user. The user in turn also benefits from the desirable IRS-multipath effect, in which it receives signal reflected from the IRS towards its direction and achieves a sum of strong signal power at its end. Another practical setting is shown in Fig. 1.7(b). In this case, IRS deployment advantage stands out, where its presence helps the user realize the benefit of the IRS reflected beam and receive the intended information despite the blockage present between it and the BS. In this scenario the user is still capable of receiving the intended information and communicating with the BS. It is worth noting that IRS technology possesses an additional advantage, that is the practicality in deployment. IRS technology can be easily mounted onto the walls of existing buildings allowing their integration into the already built-in networks, without requiring any change in the hardware of the BS or user terminals. With such convenience and potential in deploying the IRS, this technology has gained considerable attention in theoretical and practical-based research as will be highlighted in the following section.

1.2.2 State of the Art

Motivated by the remarkable advantages of IRS technology, various works on IRS-assisted system have appeared in the last year that focus on the design of the reflect beamforming matrix at the IRS to meet different objectives. In [GLCL19], the authors formulate and solve the sum-rate maximization problem for the IRS-assisted multiple-input single-output (MISO) system by jointly optimizing the active beamforming at the BS and passive reflect beamforming at the IRS. They assume the availability of perfect CSI to design the active beamforming while the reflect beamforming is designed by modeling the true channel coefficients as realizations from the sample space that is dominated by the knowledge of the imperfect CSI. In [WZ19b, WZ18], Wu *et. al.* optimize the precoding at the BS and reflect beamforming at the IRS under the criteria of minimizing the total transmit power at the BS, subject to users' individual SINR constraints. They further extend their work in [WZ19a, WZ19d] to solve a similar optimization problem under the more practical assumption that IRS elements can only apply discrete phase shifts instead of continuous phase shifts. The work in [NKC+19b] aims at maximizing the minimum SINR of an IRS-assisted MISO system in the asymptotic regime, under the scenarios where the BS-to-IRS channel matrix is a rank-one line of sight (LoS) matrix and a full-rank LoS matrix. IRSs have also found applications in [LDY+19] and [MLG+19] in UAV communication and NOMA systems respectively. Moreover, the use of IRSs to enable indoor communication in the presence of blockages has been the subject of [TSJP16, TSKJ18].

Most of the current literature on IRS-assisted systems focuses on solving optimization problems while assuming perfect channel state information (CSI) to be available at the BS and the IRS. Channel estimation is a big practical issue in IRS-assisted communication systems since the IRS elements have no radio resources of their own to send or receive pilot symbols and no signal processing capability to estimate the IRS-assisted links. Recently some works have proposed channel estimation protocols to estimate the IRS-assisted channels taking into account the radio limitations of the IRS [MJ19b, LD19, YZZ19a, CLCY19, HY19]. Least-square channel estimates based on channel training have been proposed in [MJ19b, LD19, YZZ19a] for a single-user system while channel estimation algorithms that exploit the sparsity of the cascaded channel matrix comprising

of the BS-to-IRS link and the IRS-to-user link have been proposed for a multi-user system in [CLCY19, HY19]. However, all these works only focus on developing the channel estimation protocols and do not utilize the derived estimates or algorithms in the design and analysis of the IRS-assisted downlink system. Additionally, up to the authors' knowledge, while there has been a remarkable focus on the development of beamforming optimization algorithms for IRS-assisted systems, there has been no notable work studying the performance limits of an IRS-assisted system. Although simulations results of existing works show that it is always beneficial to deploy an IRS but these conclusions need to be backed by theoretical analysis and tested in a more practical setting with imperfect CSI.

1.3 Thesis Work

In this section, we will highlight this work's main objectives and contributions, and provide a brief outline of the thesis.

1.3.1 Objectives

In light of the research gaps highlighted in the previous section, the main objectives of this work can be summarized as follows:

- Study the performance of a multi-user IRS-assisted MISO system in a Rayleigh fading environment while assuming imperfect channel information at the BS. This includes the following:
  - Derive the MMSE estimates of the channels using a protocol that takes into account the passive nature of the IRS elements.
  - Design MRT procoders at the BS for downlink transmission and formulate the corresponding downlink SINR and sum rate expressions.
- Study the downlink sum-rate performance of a multi-user IRS-assisted MISO system in an asymptotic regime, that is where the system dimensions grow large. This includes:

  - Obtain the asymptotically tight approximation of SINR and sum rate expressions under MRT precoding using random matrix theory (RMT) tools.
  - Draw insights on the impact of IRS phase shift on the overall asymptotic performance of the system.

- Provide numerical results that prove the following:
  - The derived asymptotic sum rate expression is tight even for moderate system dimensions.
  - The array gain achieved by the deployment of IRS in MISO systems while loss of IRS-beamforming gains in the asymptotic regime under Rayleigh fading environments.
  - The usefulness of IRS in interference limited scenarios.

1.3.2 Contribution

In this thesis, we consider a multi-user IRS-assisted MISO system where an IRS, comprising of N passive reflecting elements, is deployed in the LoS of an M-antenna BS to assist it in communicating K single-antenna users. We formulate the downlink signal to interference plus noise ratio (SINR) and sum rate expressions under maximum ratio transmission (MRT) precoding and the developed MMSE channel estimation protocol. Using tools from random matrix theory (RMT), we study the asymptotic performance of the IRS-assisted system by deriving the deterministic approximations of the SINR and the sum-rate, which are tight in the limit $M, N, K \to \infty$. The derived deterministic equivalents are simplified for several special cases to gain insights into the impact of M and N on the system performance. We find that the IRS phase shift values do not matter asymptotically in the perfect CSI scenario and in the scenario with imperfect CSI and no direct channel. The phase shifts do appear in terms involving the error in the estimation of the direct channel that gets propagated to the estimation of IRS-assisted links under the proposed estimation protocol, and a project gradient ascent algorithm is proposed to optimize them. However, the terms in which these phase shifts appear are actually negligible and we find that even in the general setting with imperfect CSI and both IRS-assisted and direct channels, the IRS phase shifts play no significant role asymptotically. The asymptotic performance limit derived for fixed M and K,

and growing N reveals that IRS only yields an array and no beamforming gain in the asymptotic limit. This restricts the usefulness of IRS under Rayleigh fading to noise-limited scenarios. We conclude the thesis with numerical results that show the tightness of the developed deterministic equivalents for moderate system dimensions, confirm the insights drawn from theoretical analysis about the usefulness of the IRS and highlight the high sensitivity of IRS-assisted systems to channel estimation errors.

1.3.3 Outline

The rest of the thesis will be divided as follows: Chapter 2 presents the system model, outlines the channel estimation protocol and derives the MMSE estimates as well as introduces the utilized precoding technique. Chapter 3 carries out a rigorous asymptotic analysis of the SINR and sum-rate under imperfect CSI and simplifies the derived deterministic equivalents for different operating regimes. The chapter also concludes with presenting a gradient ascent algorithm to optimize the deterministic equivalent expressions. Chapter 4 includes the simulation results that support our work. Chapter 5 concludes the thesis and provide potential future direction.

Chapter 2

IRS-Assisted MISO Systems

In this chapter we will introduce the IRS-assisted system model and propose a practical channel estimation protocol that takes into account the passive property of IRS elements. We derive the MMSE channel estimate, which BS uses to design MRT precoders for transmission. The final signal to interference and noise ratio (SINR) and sum rate expressions are also provided with insights on the effect of channel estimate quality. This chapter provides essential channel model expressions, which will help pave the way to proceeding chapters.

2.1 System Model

In this section, we present the transmission model for the considered IRS-assisted downlink multi-user MISO system. We also develop an MMSE based channel estimation protocol to obtain CSI at the BS.

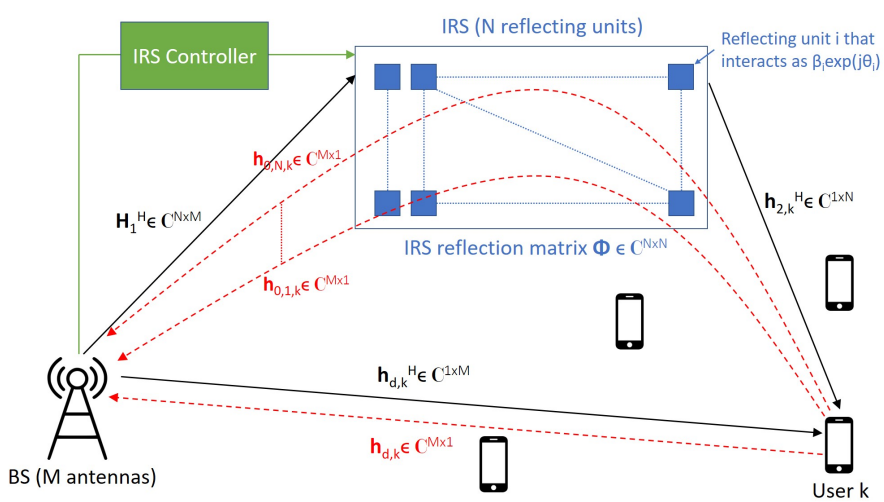

Figure 2.1: Sketch of IRS-assisted MISO system.

Signal Model

As shown in Fig. 2.1, we consider an IRS-assisted MISO communication model where a BS equipped with M antennas, communicates with K single antenna users. An IRS composed of N passive reflecting elements is installed in the LoS of the BS and assists it in communicating with the users. Equipped with a smart controller and using feedback from the BS, the IRS can dynamically adjust the phase shift induced by each reflecting element on the impinging electromagnetic waves. Additionally, we consider a time-division duplex protocol and assume transmission over quasi-static flat-fading channels. The received baseband signal y_k at user k is given as,

$$y_k = (\mathbf{h}_{d,k} + \mathbf{H}_1 \boldsymbol{\Theta} \mathbf{h}_{2,k})^H \mathbf{x} + n_k, \tag{2.1}$$

here $\mathbf{H}_1 \in \mathbb{C}^{M \times N}$ is the LoS static channel between the IRS and the BS, and $\mathbf{h}_{2,k} \sim \mathcal{CN}(\mathbf{0}, \beta_{2,k}\mathbf{I}_N) \in \mathbb{C}^{N \times 1}$ and $\mathbf{h}_{d,k} \sim \mathcal{CN}(\mathbf{0}, \beta_{d,k}\mathbf{I}_M) \in \mathbb{C}^{M \times 1}$ are the Rayleigh block fading channel vectors between user k and the IRS and user k and the BS respectively, where $\mathcal{CN}(\mathbf{m}, \mathbf{R})$ denotes the multi-variate complex Gaussian distribution with mean $\mathbf{m}$ and covariance matrix $\mathbf{R}$ and $\beta_{2,k}$, $\beta_{d,k}$ are the channel attenuation coefficients. Also $\boldsymbol{\Theta} = \text{diag}(\theta_1, \theta_2 ... \theta_N)$ represents the response of the IRS, where $\theta_n = \alpha_n \exp(j\phi_n)$, where $\phi_n \in [0, 2\pi]$ is the phase shift introduced by the element n and $\alpha_n \in [0, 1]$ is the amplitude reflection constant. Note that $\beta_{2,k}$ and $\beta_{d,k}$ are the channel attenuation coefficients for the IRS to user and BS to user links, respectively. The channel attenuation coefficient of BS to IRS link is captured in $\mathbf{H}_1$ and is represented by β_1. The channel from user k to the BS, i.e. $\mathbf{h}_k = \mathbf{h}_{d,k} + \mathbf{H}_1 \boldsymbol{\Theta} \mathbf{h}_{2,k}$ is statistically equivalent to

$$\mathbf{h}_k = \mathbf{A}_k^{1/2} \mathbf{z}_k, \tag{2.2}$$

where $\mathbf{z}_k \sim \mathcal{CN}(\mathbf{0}, \mathbf{I}_M)$ and $\mathbf{A}_k = \beta_{d,k}\mathbf{I}_M + \beta_{2,k}\mathbf{H}_1 \boldsymbol{\Theta}\boldsymbol{\Theta}^H \mathbf{H}_1^H$. Note that $\boldsymbol{\Theta}\boldsymbol{\Theta}^H = \text{diag}(\boldsymbol{\alpha})$, where $\boldsymbol{\alpha} = [\alpha_1^2, \ldots, \alpha_N^2]$. The derivation of $\mathbf{A}_k$ is provided is Appendix A.

Moreover, $\mathbf{x} = \sum_{k=1}^{K} \sqrt{p_k}\mathbf{g}_k s_k$ is the Tx signal vector, where $\mathbf{g}_k \in \mathbb{C}^{M \times 1}$, p_k and $s_k \sim \mathcal{CN}(0, 1)$ are the precoding vector, signal power and data symbol for user k respectively. The Tx vector satisfies the average Tx power per user constraint as,

$$\mathbb{E}[||\mathbf{x}||^2] = \text{tr}\,(\mathbf{P}\mathbf{G}^H\mathbf{G}) \leq P_{max}, \tag{2.3}$$

where $P_{max} > 0$ is the Tx power constraint at the BS, $\mathbf{P} = \text{diag}(p_1, \ldots, p_K)$ and $\mathbf{G} = [\mathbf{g}_1, \mathbf{g}_2, \ldots, \mathbf{g}_K] \in \mathbb{C}^{M \times K}$. The downlink SINR at user k is defined as,

$$\gamma_k = \frac{p_k |\mathbf{h}_k^H \mathbf{g}_k|^2}{\sum_{i \neq k} p_i |\mathbf{h}_k^H \mathbf{g}_i|^2 + \sigma^2}, \tag{2.4}$$

where,

$$\mathbf{h}_k = \mathbf{h}_{d,k} + \mathbf{H}_1 \mathbf{\Theta} \mathbf{h}_{2,k}, \tag{2.5}$$

denotes the overall channel between the BS and user k. The user rate is defined as,

$$R_k = \log_2(1 + \gamma_k), \tag{2.6}$$

and the sum rate is obtained as

$$R_{sum} = \sum_{k=1}^{K} \log_2(1 + \gamma_k). \tag{2.7}$$

2.2 Channel Estimation

One issue that is accompanied with the IRS technology is the channel estimation. Given the large number of elements the IRS contains, the number of links to be estimated increases. Additionally, the IRS elements are passive in nature, that is the elements lacks radio resources to undergo any signal transmission or processing, and therefore the CSI can only be estimated at the BS.

2.2.1 State of the Art

Current literature on IRS-assisted systems' channel estimation involves several promising approaches to tackling the above limitations. In [TAA19a], Taha *et al.* proposed an algorithm that uses compressive sensing and deep learning techniques to tackle the estimation problem. In their setting, some IRS elements are active and rest are passive, where the deep learning techniques and compressive sensing are used to estimate the channels of all IRS elements via active IRS units. In [HY20], He *et al.* proposed a two-stage algorithm, which includes a sparse matrix factorization stage and matrix completion stage to derive the cascaded BS-IRS and IRS-user channel estimates. The estimation is done by keeping one element (or group of elements) active at each stage of

estimation process. Another approach which involves minimum variance unbiased estimator is introduced in [JC19], where Jensen *et al.* proposed a channel estimation scheme that is based on minimizing Cramer Rao Lower Bound (CRLB) under certain constraint. You *et al.* in [YZZ19b] proposed a channel training protocol where the IRS elements are divided into M groups, such that each group shares the same reflection coefficient. The user sends an $(M + 1)$ pilot symbols to the AP, where the AP stacks the consecutive received signals and estimates the extended channel $\mathbf{h}$. Motivated by the above works, in the following section, we will propose a new and practical channel estimation protocol that basically works by turning ON one IRS element at a time while keeping the rest OFF during the training process to estimate each channel individually. The process involves estimating a total of $N + 1$ channels.

2.2.2 Proposed Protocol

Channel estimation is necessary to compute the precoding vectors at the BS and the reflect beamforming matrix $\mathbf{\Theta}$ at the IRS. The real difficulty is in the estimation of $\mathbf{H}_1$ and $\mathbf{h}_{2,k}$, since the IRS has no radio resources of its own to transmit pilot symbols that enable the BS to estimate $\mathbf{H}_1$ or to sense $\mathbf{h}_{2,k}$ using the pilot signals received from the users. Therefore, the BS has to estimate all the channels and share this information with the IRS controller. Given the passive nature of the IRS, we adopt the TDD protocol and exploit channel reciprocity in estimating the downlink channels at the BS using the received uplink pilot signals from the users. For this purpose, we divide the channel coherence period of τ sec into an uplink training phase of τ_c and a downlink transmission phase of τ_d. Throughout the uplink training phase, the users transmit mutually orthogonal pilot symbols. After correlating the received training signal with the pilot sequence of user k, the BS estimates the channel vector $\mathbf{h}_k$ based on the received observation vector $\mathbf{y}_k^{tr} \in \mathbb{C}^{M\times 1}$ [HtD13], given as,

$$\mathbf{y}_k^{tr} = (\mathbf{h}_{d,k} + \mathbf{H}_1\mathbf{\Theta}\mathbf{h}_{2,k}) + \mathbf{n}_k^{UL}, \quad k = 1, \ldots, K, \tag{2.8}$$

where $\mathbf{n}_k^{UL} \sim \mathcal{CN}(0, \frac{1}{\rho_{tr}}\mathbf{I}_M)$ is the noise in the uplink and $\rho_{tr} > 0$ is the effective training SNR. In general, ρ_{tr} depends on the pilot transmit power and the length of the pilot sequences. Here, we assume it to be a given parameter. To this end, note that with a change in variables, we can obtain,

$$\mathbf{H}_1\mathbf{\Theta}\mathbf{h}_{2,k} = \mathbf{H}_{0,k}\mathbf{v}, \tag{2.9}$$

where $\mathbf{H}_{0,k} = \mathbf{H}_1 \text{diag}(\mathbf{h}_{2,k}^T)$ and $\mathbf{v} = [\theta_1, \theta_2, \ldots, \theta_N] \in \mathbb{C}^{N\times 1}$. With this representation, we have cascaded $\mathbf{H}_1$ and $\mathbf{h}_{2,k}$ as $\mathbf{H}_{0,k} \in \mathbb{C}^{M\times N}$, where $\mathbf{H}_{0,k} = [\mathbf{h}_{0,1,k}, \ldots, \mathbf{h}_{0,N,K}]$ is a matrix of N column vectors. Each vector $\mathbf{h}_{0,i,k} \in \mathbb{C}^{M\times 1}$ (shown in red curved arrows in Fig. 2.1) can be interpreted as the channel from the user to the BS through the IRS when only element i of the IRS is ON i.e. $\alpha_i = 1, \phi_i = 0$ and $\alpha_n = 0, n \neq i$. We will focus on the MMSE estimation of $\mathbf{h}_{0,i,k}, i = 1, \ldots, N$ and $\mathbf{h}_{d,k}$ for $k = 1, \ldots, K$ at the BS. The received observation vector in (2.8) can be represented using (2.9) as,

$$\mathbf{y}_k^{tr} = (\mathbf{h}_{d,k} + \mathbf{H}_{0,k}\mathbf{v}) + \mathbf{n}_k^{UL}, \tag{2.10}$$

$$= (\mathbf{h}_{d,k} + \sum_{i=1}^{N} \mathbf{h}_{0,i,k}\theta_i) + \mathbf{n}_k^{UL}, \quad k = 1, \ldots, K, \tag{2.11}$$

where $\mathbf{h}_{0,i,k} = \mathbf{R}_{0,i,k}^{1/2}\mathbf{q}_k$. Note that $\mathbf{q}_k \sim \mathcal{CN}(0, \mathbf{I}_M)$, $\mathbf{R}_{0,i,k} = E[\mathbf{h}_{0,i,k}\mathbf{h}_{0,i,k}^H] = \beta_{2,k}\mathbf{H}_1(:,i)\mathbf{H}_1(:,i)^H$, and $\mathbf{H}_1(:,i)$ is column i of $\mathbf{H}_1$. The latter is obtained by using the fact that $\mathbf{h}_{0,i,k} = \mathbf{H}_1(:,i)\mathbf{h}_{2,k}(i)$.

The channel estimation interval is divided into $N + 1$ sub-phases of length $\tau_s = \frac{\tau_c}{N+1}$. The IRS reflecting elements are controlled such that during the first sub-interval, all IRS elements are turned OFF, i.e. $\alpha_n = 0, \forall n$. Therefore in this sub-phase the BS will only receive the pilot signals transmitted over the direct channel and will be able to estimate $\mathbf{h}_{d,k}$. In the following $(i + 1)$ sub-phases, where $i = 1, \ldots, N$, only the ith IRS element is turned ON in the full reflection mode (i.e. $\alpha_i = 1, \phi_i = 0$). Therefore in sub-phase i, the BS receives pilot symbols over the direct channel and the channel via IRS element i. This will facilitate the estimation of $\mathbf{h}_{0,i,k}$.

The received training signal in sub-phase 1 of the channel estimation phase is,

$$\mathbf{r}_{1,k}^{tr} = \mathbf{h}_{d,k} + \mathbf{n}_1^{UL}, \quad k = 1, \ldots, K. \tag{2.12}$$

The MMSE estimates of $\hat{\mathbf{h}}_{d,k}, k = 1, \ldots, K$ based on (2.12) are derived to be,

$$\hat{\mathbf{h}}_{d,k} = \mathbf{R}_{d,k}\mathbf{Q}_{d,k}\mathbf{r}_{1,k}^{tr}, \tag{2.13}$$

where $\mathbf{R}_{d,k} = \beta_{d,k}\mathbf{I}_M$, $\mathbf{Q}_{d,k} = (\beta_{d,k}\mathbf{I}_M + \frac{1}{\rho_{tr}}\mathbf{I}_M)^{-1}$ and ρ_{tr} is the training SNR. The proof of (2.13) is provided in Appendix A.2.

The received observation vector during the sub-phase $(i+1)$ of the channel estimation interval is given as,

$$\mathbf{r}_{i,k}^{tr} = \mathbf{h}_{d,k} + \mathbf{h}_{0,i,k} + \mathbf{n}_i^{UL}, \quad k = 1, \ldots, K, \; i = 1, \ldots, N. \tag{2.14}$$

Now since the BS already has the estimate of $\mathbf{h}_{d,k}$, it can subtract it from the observation vector and obtain,

$$\tilde{\mathbf{r}}_{i,k}^{tr} = \tilde{\mathbf{h}}_{d,k} + \mathbf{h}_{0,i,k} + \mathbf{n}_i^{UL}, \tag{2.15}$$

where $\tilde{\mathbf{h}}_{d,k} = \mathbf{h}_{d,k} - \hat{\mathbf{h}}_{d,k}$. The MMSE estimates of $\hat{\mathbf{h}}_{0,i,k}$ based on the observation vector in (2.15) are derived to be,

$$\hat{\mathbf{h}}_{0,i,k} = \mathbf{R}_{0,i,k}\mathbf{Q}_{i,k}\tilde{\mathbf{r}}_{i,k}^{tr}, \tag{2.16}$$

where $\mathbf{R}_{0,i,k} = \beta_{2,k}\mathbf{H}_1(:,i)\mathbf{H}_1(:,i)^H$,
$\mathbf{Q}_{i,k} = \left(\mathbf{C}^H_{\tilde{\mathbf{h}}_{d,k}\tilde{\mathbf{h}}_{d,k}} + \beta_{2,k}\mathbf{H}_1(:,i)\mathbf{H}_1(:,i)^H + \frac{1}{\rho_{tr}}\mathbf{I}_M\right)^{-1}$ and
$\mathbf{C}_{\tilde{\mathbf{h}}_{d,k}\tilde{\mathbf{h}}^H_{d,k}} = \mathbf{R}_{d,k} + \mathbf{R}_{d,k}\mathbf{Q}_{d,k}\mathbf{R}_{d,k}$. The derivation of (2.16) is provided in Appendix A.3.

Note that both $\hat{\mathbf{h}}_{d,k}$ and $\hat{\mathbf{h}}_{0,i,k}$ follow Gaussian distributions. Also under the orthogonality property of the MMSE estimates, the estimation error in the direct channel, denoted as $\tilde{\mathbf{h}}_{d,k} = \mathbf{h}_{d,k} - \hat{\mathbf{h}}_{d,k}$, follows Gaussian distribution and is uncorrelated with $\hat{\mathbf{h}}_{d,k}$ (as well as independent due to joint Gaussianity of both vectors) . Similarly, the estimation error vector in each IRS-assisted channel, denoted as $\tilde{\mathbf{h}}_{0,i,k} = \mathbf{h}_{0,i,k} - \hat{\mathbf{h}}_{0,i,k}$, also follows Gaussian distribution and is uncorrelated (and independent) with $\hat{\mathbf{h}}_{0,i,k}$. Using the results derived above, it can be easily seen that $\hat{\mathbf{h}}_k = \hat{\mathbf{h}}_{d,k} + \sum_{i=1}^N \hat{\mathbf{h}}_{0,i,k}\theta_i$ will also follow a Gaussian distribution and can be expressed as a correlated Rayleigh channel as follows.

Lemma 2.1. *The channel estimate $\hat{\boldsymbol{h}}_k = \hat{\boldsymbol{h}}_{d,k} + \sum_{i=1}^N \hat{\boldsymbol{h}}_{0,i,k}\theta_i$ can be represented as,*

$$\hat{\boldsymbol{h}}_k = \boldsymbol{C}_k^{1/2}\boldsymbol{r}_k, \tag{2.17}$$

where $\boldsymbol{r}_k \sim \mathcal{CN}(0, \boldsymbol{I}_M)$ and,

$$\boldsymbol{C}_k = \boldsymbol{R}_{d,k}\boldsymbol{Q}_{d,k}\boldsymbol{R}_{d,k} + \sum_{i=1}^N \boldsymbol{R}_{0,i,k}\boldsymbol{Q}_{i,k}\left(\beta_{2,k}\boldsymbol{H}_1(:,i)\boldsymbol{H}_1(:,i)^H + \frac{1}{\rho_{tr}}\boldsymbol{I}_M\right)\boldsymbol{Q}^H_{i,k}\boldsymbol{R}^H_{0,i,k}$$
$$+ \sum_{i=1}^N\sum_{j=1}^N \theta_i\boldsymbol{R}_{0,i,k}\boldsymbol{Q}_{i,k}\boldsymbol{C}_{\tilde{\boldsymbol{h}}_{d,k}\tilde{\boldsymbol{h}}^H_{d,k}}\boldsymbol{Q}^H_{j,k}\boldsymbol{R}^H_{0,j,k}\theta_j^*. \tag{2.18}$$

Proof. The proof of Lemma 2.1 is provided in Appendix A.4.

The derived MMSE estimates of the composite channel $\mathbf{h}_k$ can be used to design transmit precoders and to evaluate user's SINR as well as the achievable sum rate expressions. This will be further elaborated in the following section.

2.3 Beamforming and Achievable Rate

In this section, we'll use the derived MMSE channel estimates to design the maximum ratio transmission (MRT) precoder and formulate the SINR expression. The formulated expressions will note the effect of the channel estimation error on the overall achievable sum rate.

2.3.1 Maximum-Ratio Transmission Precoding

With TDD operation, BS utilizes the MMSE estimates of $\mathbf{h}_k$ from (2.17) to implement MRT precoding. By adopting MRT, the symbol of each user is precoded by the Hermitian of its channel vector. MRT reduces the computational complexity greatly as compared to RZF/ZF precoding, which involves the inversion of the Gram matrix of joint users' channel matrix. With MRT precoding, the precoding vector is given as $\mathbf{g}_k = \zeta\hat{\mathbf{h}}_k$ and the precoding matrix is given as,

$$\mathbf{G}^H = \zeta\hat{\mathbf{H}}, \tag{2.19}$$

where $\hat{\mathbf{H}} = \left[\hat{\mathbf{h}}_1, \hat{\mathbf{h}}_2, \cdots, \hat{\mathbf{h}}_K\right]^H \in \mathbb{C}^{K\times M}$, and ζ ensures that the power constraint in (2.3) is satisfied as,

$$\zeta^2 = \frac{P_{max}}{\mathrm{tr}\left(\mathbf{P}\hat{\mathbf{H}}\hat{\mathbf{H}}^{\mathrm{H}}\right)} = \frac{P_{max}}{\Psi}, \tag{2.20}$$

where $\Psi = \mathrm{tr}\left(\mathbf{P}\hat{\mathbf{H}}\hat{\mathbf{H}}^{\mathrm{H}}\right)$.

2.3.2 SINR and Achievable Rate

To compute the SINR in the downlink, the user needs to have CSI too. A well-known feature of large-scale MIMO systems is channel hardening, i.e. the effective useful channel $\mathbf{h}_k^H\mathbf{g}_k$ of a user

converges to its average value when M grows large. Hence, it is sufficient for each user to have only the statistical CSI and the resulting performance loss vanishes in the large system limit. Using this idea, an ergodic achievable user rate can be computed using a technique from [Med00], widely applied to large-scale MIMO systems [HtD13, NKDA19]. The main idea is to decompose y_k in (2.1) using the definition of $\mathbf{x}$ in Sec. II-A as $y_k = \sqrt{p_k}\mathbb{E}[\mathbf{h}_k^H\mathbf{g}_k]s_k + \sqrt{p_k}(\mathbf{h}_k^H\mathbf{g}_k - \mathbb{E}[\mathbf{h}_k^H\mathbf{g}_k])s_k + \sum_{l\neq k}\sqrt{p_l}\mathbf{h}_k^H\mathbf{g}_l s_l + n_k$ and assume that the average effective channel $\mathbb{E}[\mathbf{h}_k^H\mathbf{g}_k]$ is perfectly known at user k. By treating the interference and channel uncertainty as worst-case Gaussian noise, the user k can achieve the ergodic rate,

$$R_k = \log_2(1 + \gamma_k), \tag{2.21}$$

without knowing the instantaneous values of $\mathbf{h}_k^H\mathbf{g}_k$. The parameter γ_k can be interpreted as the effective average downlink SINR of user k and is defined under MRT as,

$$\gamma_k = \frac{p_k\mathbb{E}[|\mathbf{h}_k^H\hat{\mathbf{h}}_k|^2]}{p_k\mathrm{var}[\mathbf{h}_k^H\hat{\mathbf{h}}_k] + \sum_{l\neq k} p_l\mathbb{E}[|\mathbf{h}_k^H\hat{\mathbf{h}}_l|^2] + \frac{\Psi}{\rho}}, \tag{2.22}$$

where $\rho = \frac{P_{max}}{\sigma^2}$. The ergodic achievable sum rate is given as:

$$R_{sum} = \sum_{k=1}^{K}\log_2(1 + \gamma_k). \tag{2.23}$$

2.4 Discussion

In this chapter we derived the MMSE estimate of the composite channel $\mathbf{h}_k$ through a proposed protocol that involves estimating $N + 1$ channels. More precisely, N channels account for the channels between the BS and user k via the i'th IRS element for $i = 1 \ldots N$, and one direct channel accounts for the channel between the BS and user k. Therefore the composite channel estimate $\hat{\mathbf{h}}_k = \hat{\mathbf{h}}_{d,k} + \sum_i^N \hat{\mathbf{h}}_{0,i,k}\theta_i$ relies on the $N + 1$ channel estimates to compute. Once the BS computes the composite MMSE channel estimate $\hat{\mathbf{h}}_k$, it utilizes linear processing technique to design MRT precoders, which help optimize the performance gain at the user and leverage the benefits of MIMO systems as explained in section 1.1.3. Under the channel hardening effect, user's SINR expression can be expressed as in (2.22)

It is important to note the effect of the channel estimate accuracy on the overall system's performance. As shown in (2.23), the sum rate depends on the SINR at user terminals, whose value in turn depends on the channel estimate $\hat{\mathbf{h}}_k$. Therefore, the channel estimation technique and the estimate quality play a major role in the SINR achieved at user terminal k. In fact, considering the SINR expression in (2.22), we can note the effect of the power of channel estimation error in the denominator terms, $\mathrm{var}[\mathbf{h}_k^H \hat{\mathbf{h}}_k]$ and $\sum_{l \neq k} p_l \mathbb{E}[|\mathbf{h}_k^H \hat{\mathbf{h}}_l|^2]$, where a dominating error power can significantly drop the system's performance.

Additionally by considering the expression in (2.22) in the asymptotic limit, the effective average downlink SINR can be analyzed under an asymptotic regime and expressed as a deterministic equivalent. These expressions can be very useful to solve optimization problems as will be seen in the following chapter.

Chapter 3

Asymptotic Analysis

In this section we derive the deterministic approximations of users' SINR and ergodic rate expressions under MRT precoding for IRS assisted systems [WZ18, NKC+19b, MLG+19, TAA19b]. This assumption seems realistic with the advancement in the design and fabrication of loss-less meta-surfaces [BMR17, EE16]. Section 3.1 provides a brief motivation behind studying the asymptotic performance of the wireless system followed with some useful lemmas utilized in our work. Section 3.2 will provide the assumptions made and the derived expressions.

3.1 Motivation and Useful Lemmas

An important performance metric in communication systems is the users' ergodic rates, which are generally difficult to study for finite system dimensions. In fact, the SINR expression in (2.22) yields no insights into the performance of the system. With the advent of 5G technology and the deployment of large-dimension networks to serve multiple users, the network performance analysis under the asymptotic regime has become an area of interest. In the large M, N, K regime, the users' SINRs and ergodic rates tend to approach deterministic quantities. These quantities depend only on the statistics of the channels and are referred to as deterministic equivalents. These deterministic equivalents are almost surely (a.s.) tight in the asymptotic limit, i.e. as the system dimensions grow to infinity, the approximations yielded by these deterministic equivalents tend to the actual values with probability one. These equivalents depend only on the statistics of the channel and are very useful to solve important optimization problems as studied in [WCDS12a, HtD13, NKDA19, NKC+19b]. Given the resulting optimization solutions rely only on the knowledge of channel's large-scale statistics which vary very slowly, so solving the optimization problems at the pace of fast fading is not required.

Under this motivation, we exploit the statistical distribution of $\mathbf{h}_k$ and large values of M, N, K to

compute the deterministic approximations of user's SINR and ergodic rates. These approximations will yield very important insights into how the presence of IRS impacts the performance of the system.

The derivations in this section will exploit the following lemmas.

Lemma 3.1. *Let $\boldsymbol{A} \in \mathbb{C}^{N\times N}$ and $\boldsymbol{x} \in \mathbb{C}^{N\times 1}$ be a random vector of i.i.d entries independent of $\boldsymbol{A}$. Assume the components of $\mathbf{x}$ have mean zero, variance 1 and $\boldsymbol{A}$ satisfies $\limsup_N ||\boldsymbol{A}|| < \infty$. Then,*

$$\frac{1}{N}\boldsymbol{x}^H\boldsymbol{A}\boldsymbol{x} - \frac{1}{N}tr(\boldsymbol{A}) \xrightarrow[N\to\infty]{a.s} 0. \tag{3.1}$$

Lemma 3.2. *Let $\boldsymbol{A}$ be as defined in lemma 3.1 and $\boldsymbol{x}$ and $\boldsymbol{y}$ be i.i.d vectors with the same distribution as defined in lemma 3.1 as well. Then,*

$$\frac{1}{N}\boldsymbol{x}^H\boldsymbol{A}\boldsymbol{y} \xrightarrow[N\to\infty]{a.s} 0. \tag{3.2}$$

Lemma 3.3. *Let $\boldsymbol{A}_1, \boldsymbol{A}_2 \ldots$ be an infinite sequence of matrices with $\boldsymbol{A}_N \in \mathbb{C}^{N\times N}$, be deterministic with bounded spectral norm and $\boldsymbol{B}_1, \boldsymbol{B}_2 \ldots$ with $\boldsymbol{B}_N \in \mathbb{C}^{N\times N}$, be random Hermitian with eigenvalues $\lambda_1^{\boldsymbol{B}_N} \leq \lambda_2^{\boldsymbol{B}_N} \cdots \leq \lambda_N^{\boldsymbol{B}_N}$ such that with probability 1, there exists $\varepsilon > 0$ for which $\lambda_1^{\boldsymbol{B}_N} > \varepsilon$ for all large N. Then for $\boldsymbol{v} \in \mathbb{C}^N$*

$$\frac{1}{N}tr\boldsymbol{A}_N\boldsymbol{B}_N^{-1} - \frac{1}{N}tr\boldsymbol{A}_N(\boldsymbol{B}_N + \boldsymbol{v}\boldsymbol{v}^H)^{-1} \xrightarrow[N\to\infty]{a.s} 0. \tag{3.3}$$

One intuitive way to look at the above lemmas is to relate it to the law of large numbers (LLN). For simplicity, let us consider $\mathbf{A}$ be an identity matrix, i.e. $\mathbf{A} = \mathbf{I}_N$. By the LLN, $\mathbf{x}^H\mathbf{A}\mathbf{x}$ approaches $\mathbb{E}[\mathbf{x}^H\mathbf{A}\mathbf{x}]$ as $N \to \infty$. For a finite N,we can show that $\mathbb{E}[\mathbf{x}^H\mathbf{A}\mathbf{x}] = \frac{1}{N}tr(\mathbf{A})$ [CD11], which is equivalent to saying $\mathbb{E}[\mathbf{x}^H\mathbf{I}_N\mathbf{x}] = \frac{1}{N}tr(\mathbf{I}_N)$ for the simplified scenario, where $tr(\mathbf{I}_N)$ is the sum of x entries variances. Therefore, lemma 3.1 can be concluded. A similar approach can be taken when looking at lemma 3.2. The above lemmas and their rigorous proofs can be found in [CD11, TV04]

3.2 Deterministic Equivalence Results

The main theorem proposed in this section and the corollaries that follow are the major contributions of this work as they use the IRS-assisted channel in (2.2) and its estimate in (2.17) to derive

the deterministic approximation of each user's SINR under MRT precoding. Before we introduce these results, we will require the following assumptions:

Assumption 1. M, N and K grow large with a bounded ratio as $0 < \liminf_{M,K\to\infty} \frac{K}{M} \leq \limsup_{M,K\to\infty} \frac{K}{M} < \infty$ and $0 < \liminf_{M,N\to\infty} \frac{M}{N} \leq \limsup_{M,N\to\infty} \frac{M}{N} < \infty$.

Assumption 2. The LoS channel matrix $\mathbf{H}_1$ satisfies,

$$\limsup_{M\to\infty} ||\mathbf{H}_1\mathbf{H}_1^H|| < \infty. \tag{3.4}$$

Assumption 3. The entries of the power matrix $\mathbf{P} = \text{diag}(p_1, p_2, \ldots, p_K)$ are of order $O(1/K)$.

The above assumptions are needed to help ensure a bounded norm on channel matrix, dimension ratio and power as the system's dimensions grow. This is required in the derivation of the deterministic equivalents of the SINR and sum rate to ensure a bounded limit and tight approximation as system grows large.

We now present the deterministic equivalent of the SINR of user k defined in (2.22) in the following Theorem.

3.2.1 IRS Assisted System with a Direct Channel

In this subsection we will provide the deterministic equivalents of the SINR and sum expressions of an IRS-assisted system with a composite channel comprised of both an IRS-assited channel and a direct channel, as shown in Fig. 2.1.

Theorem 3.1. *Under Assumptions 1, 2 and 3, the SINR of user k defined in (2.22), for the channel in (2.2) and its estimate in (2.17) converges as,*

$$\gamma_{k,MRT} - \gamma^{\circ}_{k,MRT} \xrightarrow[M,N,K\to\infty]{a.s} 0, \tag{3.5}$$

where $\gamma^{\circ}_{k,MRT}$ is defined as:

$$\gamma^{\circ}_{k,mrt} = \frac{\frac{p_k}{K}|\sum_{i=1}^{N}\theta_i tr(\boldsymbol{C}_{\tilde{\boldsymbol{h}}_{d,k}\tilde{\boldsymbol{h}}_{d,k}}\boldsymbol{R}_{0,i,k}\boldsymbol{Q}_{i,k}) + \frac{\beta_{d,k}^2 M}{\beta_{d,k}+\frac{1}{\rho tr}} + \sum_{i=1}^{N} tr(\boldsymbol{R}_{0,i,k}\boldsymbol{R}_{0,i,k}\boldsymbol{Q}_{i,k})|^2}{\sum_{l\neq k}\frac{p_l}{K}tr(\boldsymbol{C}_l\boldsymbol{A}_k) + \frac{\frac{p_k}{K}\sum_{k=1}^{K} tr\boldsymbol{C}_k}{\rho}}, \tag{3.6}$$

where $\mathbf{A}_k = \beta_{2,k}\mathbf{H}_1\mathbf{H}_1^H + \beta_{d,k}\mathbf{I}_M$ and $\boldsymbol{C}_l$ is defined in Lemma 2.1 in (2.18).

Proof. The proof of Theorem 3.1 is provided in Appendix B

Two important insights can be drawn from the expression in (3.6). First, the phase shifts applied by the IRS elements, i.e. $v_n = \exp(j\theta_n)$, do not appear anywhere except for the terms involving the MMSE covariance matrix $\mathbf{C}_{\tilde{\mathbf{h}}_{d,k}\tilde{\mathbf{h}}_{d,k}}$ of $\mathbf{h}_{d,k}$. The error in the estimation of $\mathbf{h}_{d,k}$s propagates in the estimation of the subsequent $\mathbf{h}_{0,i,k}$s under the proposed protocol as shown in (2.16) making $\mathbf{h}_{d,k}$ and $\tilde{\mathbf{r}}^{tr}_{i,k}$, $i = 1, \ldots, N$ dependent due to the presence of $\tilde{\mathbf{h}}_{d,k}$ in $\tilde{\mathbf{r}}^{tr}_{i,k}$. If the direct channel is estimated accurately, the phase shifts will not matter asymptotically in an IRS-assisted system and IRS will not yield any reflect beamforming gain. This phenomenon is caused by the spatial isotropy that holds upon the IRS-assisted channel, which is insensitive to the beamforming between $\mathbf{H}_1$ and $\mathbf{h}_{2,k}$ under Rayleigh fading $\mathbf{h}_{2,k}$s[1]. Second, the IRS can still yield an array gain due to the sum of N contributions of the IRS elements in the numerator. However, there are also some terms with sum of N contributions of the IRS elements in the denominator. We will see whether the IRS gain in the desired signal energy is larger than the gain in the interference in subsection 3.21 .

In the next corollary, we present the deterministic equivalents of the users' ergodic rates in (2.21).

Corollary 3.1. *Assume that Assumption 1, 2 and 3 hold true. From the continuous mapping theorem it follows that the individual downlink rates R_k of the users converge as,*

$$R_k - R_k^{\circ} \xrightarrow[M,N,K\to\infty]{a.s} 0, \tag{3.7}$$

where,

$$R_k^{\circ} = \log(1 + \gamma_k^{\circ}), \tag{3.8}$$

where γ_k° is given by (3.6).

[1]The same conclusion holds if both $\mathbf{H}_1$ and $\mathbf{h}_{2,k}$ undergo Rayleigh fading.

An approximation for the average sum rate can be obtained as follows:

$$R^{\circ}_{sum} = \sum_{k=1}^{K} \log(1 + \gamma^{\circ}_{k}), \tag{3.9}$$

such that,

$$\frac{1}{K}(R_{sum} - R^{\circ}_{sum}) \xrightarrow[M,N,K\to\infty]{a.s} 0. \tag{3.10}$$

The next subsection considers the special case where the direct channel from the BS to the user is blocked.

3.2.2 IRS Assisted System with a Blocked Direct Channel

Let us now consider an IRS assisted transmission scenario in Fig. 2.1, where the direct channel is blocked, i.e. $\mathbf{h}_{d,k} = 0$. For such a scenario, the channel model in (2.2) is simplified to,

$$\mathbf{h}_k = \mathbf{H}_1 \mathbf{\Theta} \mathbf{h}_{2,k}. \tag{3.11}$$

The channel can be equivalently written as,

$$\mathbf{h}_k = \mathbf{A}_k^{1/2} \mathbf{z}_k, \tag{3.12}$$

where $\mathbf{z}_k \sim \mathcal{CN}(\mathbf{0}, \mathbf{I}_M)$ and $\mathbf{A}_k = \beta_{2,k} \mathbf{H}_1 \mathbf{H}_1^H$.

The channel estimation phase will only have N sub-phases where the IRS elements are switched ON one-by-one. There is no estimation of the direct channel involved and the estimates of $\mathbf{h}_{0,i,k}$, $i = 1, \ldots, N$ in (2.16) are simplified as,

$$\hat{\mathbf{h}}_{0,i,k} = \mathbf{R}_{0,i,k} \mathbf{Q}_{i,k} \mathbf{r}^{tr}_{i,k}, \tag{3.13}$$

where $\mathbf{R}_{0,i,k}$ is the same as defined in Section II-B, $\mathbf{r}^{tr}_{i,k} = \mathbf{h}_{0,i,k} + \mathbf{n}^{UL}_i$ and $\mathbf{Q}_{i,k} = \Big(\beta_{2,k} \mathbf{H}_1(:,i) \mathbf{H}_1(:,i)^H + \frac{1}{\rho_{tr}} \mathbf{I}_M\Big)^{-1}$.

Moreover the channel estimate $\hat{\mathbf{h}}_k = \sum_{i=1}^{N} \hat{\mathbf{h}}_{0,i,k} \theta_i$ can be represented as,

$$\hat{\mathbf{h}}_k = \mathbf{C}_k^{1/2} \mathbf{r}_k, \tag{3.14}$$

where $\mathbf{r}_k \sim \mathcal{CN}(0, \mathbf{I}_M)$ and,

$$\mathbf{C}_k = \sum_{i=1}^{N} \mathbf{R}_{0,i,k} \mathbf{Q}_{i,k} \mathbf{R}_{0,i,k}. \tag{3.15}$$

The deterministic equivalent of the SINR defined in (2.22) is presented in the following Corollary.

Corollary 3.2. *Let Assumption 1, 2 and 3 hold true. Then the SINR of user k defined in (2.22), for the channel in (3.11) and its estimate in (3.14) converges as,*

$$\gamma_{k,MRT} - \gamma^{\circ}_{k,MRT} \xrightarrow[M,N,K\to\infty]{a.s} 0, \tag{3.16}$$

where $\gamma^{\circ}_{k,MRT}$ is defined as:

$$\gamma^{\circ}_{k,MRT} = \frac{\frac{1}{K} p_k |tr\boldsymbol{C}_k|^2}{\frac{1}{K}\sum_{l\neq k} p_l tr\boldsymbol{C}_l \boldsymbol{A}_k + \frac{\frac{p_k}{K}\sum_{k=1}^{K} tr\boldsymbol{C}_k}{\rho}}, \tag{3.17}$$

where $\boldsymbol{C}_k = \sum_{i=1}^{N} \boldsymbol{R}_{0,i,k}\boldsymbol{Q}_{i,k}\boldsymbol{R}_{0,i,k}$ and $\boldsymbol{A}_k = \beta_{2,k}\boldsymbol{H}_1\boldsymbol{H}_1^H$.

Notice that due to the lack direct channel between the BS and user terminal, the IRS phase shifts, which appeared along side the direct channel error in Theorem 3.1, do not show up under this setting. Consequently, in an asymptotic regime we obtain no beamforming gains under Rayleigh fading channel with blocked direct channel.

3.2.3 IRS Assisted System Under Perfect CSI

Finally, we simplify the result in Theorem 3.1 for the scenario where perfect CSI is available at the BS about all the IRS-assisted channels as well as the direct channels. The result is provided in the following corollary.

Corollary 3.3. *Under the setting of Theorem 3.1, let perfect CSI be available. Then,*

$$\gamma^{\circ}_{k,MRT} = \frac{\frac{p_k}{K}|tr(\boldsymbol{A}_k)|^2}{\sum_{l\neq k} tr(\frac{p_l}{K}\boldsymbol{A}_l\boldsymbol{A}_k) + \frac{\frac{p_k}{K}\sum_{k=1}^{K} tr(\boldsymbol{A}_k)}{\rho}}, \tag{3.18}$$

where $\boldsymbol{A}_k = \beta_{d,k}\boldsymbol{I}_M + \beta_{2,k}\boldsymbol{H}_1\boldsymbol{H}_1^H$.

Proof. The proof follows by letting $\rho_{tr} \to \infty$ in Theorem 3.1.

Under this simplified setting where perfect CSI is known at the BS, IRS phase shifts also provided no beamforming gain asymptotically. Notice that we have the direct channel in this setting, but as shown in Theorem 3.1, phases only appear with the terms involving the MMSE covariance matrix of direct channel error $\tilde{\mathbf{h}}_{d,k}$.
In the following subsection, we will consider a simplified model of the channel to gain more insights on the benefits of IRS in system's performance.

3.2.4 Special Case

To gain more explicit insights into the impact of IRS on the system performance, we consider a simplified model from [HtD13] for the channel in (2.1). Before presenting the simplified model, note that (2.1) is statistically equivalent to

$$\mathbf{h}_k = \sqrt{\beta_{d,k}}\mathbf{z}_{B,k} + \sqrt{\beta_{2,k}}(\mathbf{H}_1\mathbf{H}_1^H)^{1/2}\mathbf{z}_{I,k} = \mathbf{A}_k^{1/2}\mathbf{z}_k, \tag{3.19}$$

where $\mathbf{A}_k = \beta_{2,k}\mathbf{H}_1\mathbf{H}_1^H + \beta_{d,k}\mathbf{I}_M$, $\mathbf{z}_{B,k} \sim \mathcal{CN}(\mathbf{0}, \mathbf{I}_M)$, $\mathbf{z}_{I,k} \sim \mathcal{CN}(\mathbf{0}, \mathbf{I}_M)$ and $\mathbf{z}_k \sim \mathcal{CN}(\mathbf{0}, \mathbf{I}_M)$ [2]. We will focus on the perfect CSI scenario in this section for analytical tractability noting that it acts an an upper bound on how well the IRS-assisted system can perform under CSI errors. The deterministic equivalent for the channel in (2.2) under MRT precoding and perfect CSI has been derived in corollary 3.3.

Similar to [HtD13] which derives asymptotic performance limits of a conventional massive MISO system, we consider a simplified channel model for $\mathbf{h}_k$ given as,

$$\mathbf{h}_k = \sqrt{\beta_{d,k}}\mathbf{z}_{B,k} + \sqrt{c\beta_{d,k}}(\mathbf{D}\mathbf{D}^H)^{1/2}\mathbf{z}_{I,k}, \tag{3.20}$$

where $\mathbf{D} = \sqrt{N}\mathbf{U}$ and $\mathbf{U} \in \mathbb{C}^{M\times N}$ is composed of $M \leq N$ rows of an arbitrary $N \times N$ unitary matrix. This model basically abstracts $\mathbf{H}_1\mathbf{H}_1^H$ as $\mathbf{D}\mathbf{D}^H$ and since each diagonal entry of $\mathbf{H}_1\mathbf{H}_1^H$ is the sum of N exponential terms of norm 1 scaled by β_1, so we have introduced the normalization $\sqrt{N}$ in $\mathbf{D}$ to ensure the variance of each element of IRS-assisted channel vector stays $N\beta_1$. Moreover, we

[2]The covariance matrix for IRS-assisted channel is obtained as $\mathbb{E}[\mathbf{H}_1\mathbf{\Theta}\mathbf{h}_{2,k}\mathbf{h}_{2,k}^H\mathbf{\Theta}^H\mathbf{H}_1^H] = \beta_{2,k}\mathbf{H}_1\mathbf{H}_1^H$, by noting that $\mathbf{\Theta}\mathbf{\Theta}^H = diag(\boldsymbol{\alpha}) = \mathbf{I}_N$ under the assumption $\boldsymbol{\alpha} = [\alpha_1, \ldots, \alpha_N]^T = \mathbf{1}_N$.

have let $\beta_1\beta_{2,k} = c\beta_{d,k}, \forall k$ [3]. The channel in (3.20) is equivalent to writing $\mathbf{h}_k = \bar{\mathbf{D}}_k^{1/2}\mathbf{z}_k$, where $\mathbf{z}_k \sim \mathcal{CN}(\mathbf{0}, \mathbf{I}_M)$ and $\bar{\mathbf{D}}_k = \beta_{d,k}(c\mathbf{D}\mathbf{D}^H + \mathbf{I}_M)$. This is indeed a special case of (2.2).

Under this model, the total energy of the channel grows linearly with M and N, since $\mathbb{E}[\mathbf{h}_k^H\mathbf{h}_k] = \text{tr}\,(\bar{\mathbf{D}}_k) = \beta_{d,k}(cMN + M)$. The motivation behind this channel model is twofold. First, it assumes the antenna aperture to increase with each additional antenna element and IRS, which is in contrast to existing works which assume more and more elements to be packed into a fixed volume. An insufficiency of this channel model is that the captured energy grows without bounds as M or N grow large. However, linear energy gains can be achieved up to very large numbers of antennas if the size of the antenna array is scaled accordingly as discussed in [HtD13]. Second, the model will allow us to explicitly study the impact of the IRS on the asymptotic system performance with the only difference between (2.2) and (3.20) being that we have assumed rows of $\mathbf{H}_1$ to be orthogonal to each other. The LoS channel matrix $\mathbf{H}_1$ can be designed in practice to achieve this orthogonality and therefore the model in (3.20) can actually be realized in practice. The performance obtained using (3.20) is an upper-bound to the actual performance under (2.2). However, the insights that we obtain using this model in the rest of this section will also hold under (2.2) and imperfect CSI as will be shown in simulations.

The performance of the IRS-assisted system under perfect CSI in Corollary 3.3 can be given in a compact form closed form for the model in (3.20) as follows.

Corollary 3.4. *For the channel model (3.20) and $p_k = \frac{1}{K}, \forall k$, $\gamma^{\circ}_{k,MRT}$ in Corollary 3.3 is given as,*

$$\gamma^{\circ}_{k,MRT} = \frac{1}{\underbrace{\frac{1}{M}\sum_{l\neq k}\frac{\beta_{d,l}}{\beta_{d,k}}}_{Interference} + \underbrace{\frac{\sum_{l=1}^{K}\beta_{d,l}}{M\beta_{d,k}^2\rho(cN+1)}}_{Noise}}. \tag{3.21}$$

The proof of Corollary 3.4 is provided in Appendix C.

The resulting expression captures the interference caused by the system as well as the noise experienced by the system, where both effects are normalized by the desired signal power. This corollary yields two very important insights. First it verifies the “massive MIMO effect" observed in [HtD13], which means that as M increases for fixed N and K, the SINR and therefore the user rates grows unboundedly.

[3]This assumption is justified in scenarios where IRS is located very close to the BS. In such cases, c will account for the fixed extra loss that occurs in the IRS-assisted link.

Second, the use of an IRS in Rayleigh fading environments is *only* useful when the average received SNR is low, i.e. either the noise level is high or the path losses are very high (i.e. the values of β_1 and $\beta_{2,k}$ are low). In such a noise-limited scenario, the second term in the denominator of (3.21) will dominate over the first and increasing N will produce a noticeable decrease in the noise and increase in the SINR values. In an interference-limited scenario, i.e. where the first term in the denominator of (3.21) dominates over the second, the use of an IRS yields no substantial benefit. This can be intuitively explained by noting that in Rayleigh fading channels, the phases of the IRS do not matter and all the IRS does is provide an array gain of N. This array gain appears in both the energy of the desired signal as well as the energy of the interfering signal and thereby the net effect is negligible if the denominator of the SINR is dominated by the interference. Therefore, the use of an IRS in Rayleigh fading environments will only be beneficial in noise-limited scenarios, for example, where users are located at cell edges such that the path loss is very high.

It will be interesting to study the performance of the IRS-assisted system under Rician fading channels, there is a strong LoS component from IRS to user. Under such a setting, the values of phase-shifts will matter and the IRS will yield a reflect beamforming gain where reflect beamforming can be designed to minimize the interference term. However, this is outside the scope of the current work as our focus is to gauge the practicality of using an IRS in the commonly studied Rayleigh fading environments in existing works on IRS.

3.3 Reflect-Beamforming for Performance Optimization

We have already seen that the values of the phase shifts applied by the IRS elements do not matter in Rayleigh fading environments under perfect CSI. Moreover they also do not appear in the asymptotic expression of the SINR under imperfect CSI when the direct BS-to-user channel is absent. Under the proposed channel estimation protocol, the elements of $\mathbf{v}$ do appear in the deterministic equivalent of the SINR in (3.6) in Theorem 3.1 in the terms related to the error in the estimation of $\mathbf{h}_{d,k}$ propagated to the estimation of $\mathbf{h}_{0,i,k}$, $i = 1, \ldots, N$. Therefore, even though asymptotically the IRS elements do not need to be optimized under Rayleigh fading environments, but under the proposed channel estimation protocol we can minimize the channel estimation error in $\hat{\mathbf{h}}_{d,k}$ propagated to the estimation of IRS-assisted channels by solving the following optimization

problem.

$$(P1) \qquad \max_{\theta_1,\ldots,\theta_N} \quad R^{\circ}_{sum} = \sum_{k=1}^{K} \log(1+\gamma^{\circ}_k) \tag{3.22a}$$

$$\text{s.t.} \qquad |\theta_n| = 1, \ \ \forall n. \tag{3.22b}$$

(P1) is a constrained maximization problem that can be solved using projected gradient ascent to increase the objective function by taking iterative steps proportional to the positive gradient. In each step we project the solution to the closest feasible point that satisfies the constraint in (3.22b). The algorithm is explained in Algorithm 1. To proceed, we need to the derivative of R°_{sum} with respect to each θ_n, $n = 1, \ldots N$ which is stated in the following lemma.

Lemma 3.4. *The derivative of R°_{sum} defined in 3.6 with respect to θ_n is given as*

$$\frac{\partial R^{\circ}_{sum}}{\partial \theta_n} = \sum_{k=1}^{K} \frac{1}{(1+\gamma^{o}_k)\ln(2)} \frac{2d_k \frac{p_k}{K}|n_k| tr(\boldsymbol{C}_{\tilde{\boldsymbol{h}}_{d,k}\tilde{\boldsymbol{h}}_{d,k}} \boldsymbol{R}_{0,n,k}\boldsymbol{Q}_{n,k}) - \frac{p_k}{K}|n_k|^2 d'_k}{d_k^2}, \tag{3.23}$$

where,

$$n_k = \sum_{i=1}^{N} \theta_i tr(\boldsymbol{C}_{\tilde{\boldsymbol{h}}_{d,k}\tilde{\boldsymbol{h}}_{d,k}} \boldsymbol{R}_{0,i,k}\boldsymbol{Q}_{i,k}) + \frac{\beta^2_{d,k} M}{\beta_{d,k} + \frac{1}{\rho_{tr}}} + \sum_{i=1}^{N} tr(\boldsymbol{R}_{0,i,k}\boldsymbol{R}_{0,i,k}\boldsymbol{Q}_{i,k}), \tag{3.24}$$

$$d_k = \sum_{l\neq k} \frac{p_l}{K} tr(\boldsymbol{C}_l \boldsymbol{A}_k) + \frac{p_k}{K\rho} \sum_{k=1}^{K} tr\boldsymbol{C}_k, \tag{3.25}$$

$$\begin{aligned} d'_k = 2\sum_{i=1}^{N} \theta_i (\sum_{l\neq k} \frac{p_l}{K} tr(\mathbf{R}_{0,i,l}\mathbf{Q}_{i,l}\mathbf{C}_{\tilde{\boldsymbol{h}}_{d,l}\tilde{\boldsymbol{h}}_{d,l}} \mathbf{Q}^H_{n,l}\mathbf{R}^H_{0,n,l}\mathbf{A}_k) + \\ \sum_{k=1}^{K} \frac{p_k}{K\rho} tr(\mathbf{R}_{0,i,k}\mathbf{Q}_{i,k}\mathbf{C}_{\tilde{\boldsymbol{h}}_{d,k}\tilde{\boldsymbol{h}}_{d,k}} \mathbf{Q}^H_{n,k}\mathbf{R}^H_{0,n,k})). \end{aligned} \tag{3.26}$$

Proof. The poof of lemma 3.4 is provided in Appendix D

We denote the IRS phase-shifts vector as $\mathbf{v}^s = [\theta^s_1, \theta^s_2, \ldots, \theta^s_N]$, where θ^s_n is the nth IRS element response at step s of the algorithm. The adopted gradient ascent direction is denoted as $\mathbf{p}^s$, where $[\mathbf{p}^s]_n = \frac{\partial R^o_{sum}}{\partial \theta_n}|_{\theta^s_n}$. The next step updates the phase-shifts vector in a step proportional to the positive gradient as $\tilde{\mathbf{v}}^{s+1} = \mathbf{v}^s + \mu \mathbf{p}^s$, where the step size μ is obtained using backtracking line search [BV04]. The solution $\tilde{\mathbf{v}}^{s+1}$ is projected onto the closest feasible point that satisfies the constraint (3.22b) as

Algorithm 1: Projected Gradient Ascent Algorithm for the IRS Design

procedure DESIGN OF IRS PHASE-SHIFTS VECTOR($\mathbf{v}^*$)
  Initialize: $\mathbf{v}^1 = \exp(j\pi/2)\mathbf{1}_N$, $R_{sum}^{\circ^1} = f(\mathbf{v}^1)$ given by (3.9), $\epsilon > 0$.
  set s=1;
  Repeat
  $[\mathbf{p}^s]_n = \frac{\partial R_{sum}^{\circ}}{\partial \theta_n}|_{\theta_n^s}$, $n = 1, \ldots, N$, where $\frac{\partial R_{sum}^{o}}{\partial \theta_n}$ is given in (3.23);
  μ=backtrack line search($f(\mathbf{v}^s)$, $\mathbf{p}^s$, $\mathbf{v}^s$) [BV04];
  $\tilde{\mathbf{v}}^{s+1} = \mathbf{v}^s + \mu \mathbf{p}^s$;
  $\mathbf{v}^{s+1} = \exp(j\arg(\tilde{\mathbf{v}}^{s+1}))$;
  $R_{sum}^{o^{s+1}} = f(\mathbf{v}^{s+1})$;
  Update $s = s + 1$;
  Until $||R_{sum}^{o^{s+1}} - R_{sum}^{o^s}||^2 < \epsilon$; Obtain $\mathbf{v}^* = \mathbf{v}^{s+1}$;

$\mathbf{v}^{s+1} = \exp(j\arg(\tilde{\mathbf{v}}^{s+1}))$. The complete algorithm is outlined in Algorithm 1.

As one might expect, optimizing the IRS phase-shifts provides a very small gain in the sum-rate performance as will be seen in the simulations since the phase-shifts appear only in terms involving the error covariance matrix $\mathbf{C}_{\tilde{\mathbf{h}}_{d,k}\tilde{\mathbf{h}}_{d,k}}$, which are almost negligible. Nevertheless, developing a gradient ascent algorithm for the phase shifts that appear in the asymptotic expression in Theorem 3.1 under the ON/OFF channel estimation protocol might be beneficial in scenarios where the error in the estimation of direct channel is high.

3.4 Conclusion and Discussion

In this chapter, the asymptotic performance of an IRS-assisted system was studied under various cases to gain an insight on the benefit of IRS-assisted communication. Specifically, we derived the deterministic equivalence of the SINR and sum rate expressions, and drew conclusions on the effect of IRS phase shifts in the overall performance of the system in an asymptotic regime. We were able to conclude that an IRS-assisted system operating in large dimensions under Rayleigh fading environment, whose direct channel between the BS and user is blocked, does not benefit from

beamforming gains, since IRS phase shift values do not appear in the asymptotic equivalences. Same conclusion can be drawn for the case where perfect CSI is known while direct channel between BS and user exists. Nevertheless, in the case where imperfect CSI is considered and direct channel is present, the IRS phase shifts do appear but only in terms related to the error of the direct channel estimation. These conclusions are important to asses the performance of large dimension wireless network in a Rayleigh block fading environment with an IRS deployed to assist in communication. To provide more visual results, the next chapter help support our conclusions by providing numerical results and simulations that prove the tightness of the derived deterministic equivalences under large dimensions as well as analyze the IRS-assisted system performance under optimized phase shifts with comparison to conventional MISO systems.

Chapter 4

Numerical Analysis

This chapter provides simulation results that (i) validate the derived deterministic approximation of the SINR for large dimensional systems, provide (ii) insights on the size of IRS needed to provide competing achievable sum rate performance as compared to conventional MISO systems at a lower cost of implementation, and (iii) useful insights on the performance limit of IRS-assisted systems under varying cell radius.

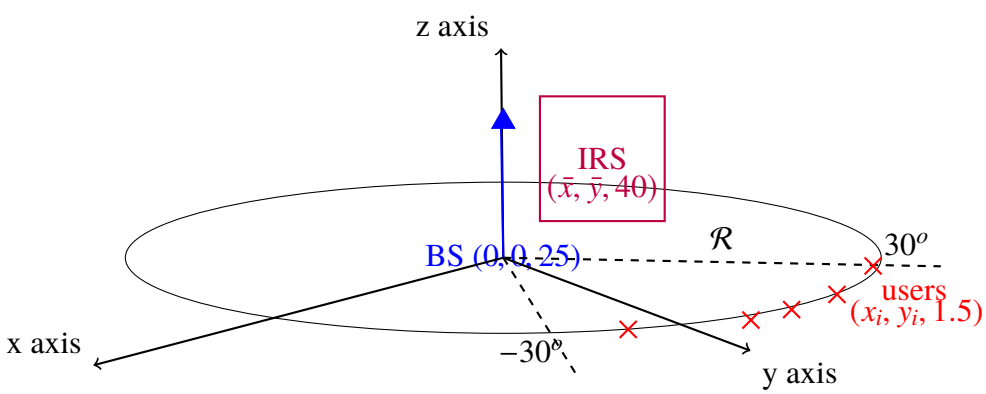

Figure 4.1: Multiuser IRS-assisted system setup

In our simulations model we consider a 3D coordinate system with a linear array of antennas at the BS and passive reflecting elements at the IRS. The coordinates of the BS, IRS and user are denoted as $(x_{BS}, y_{BS}, 25)$, $(x_{IRS}, y_{IRS}, 40)$, $(x_U, y_U, 1.5)$, respectively. We assume a full rank BS-to-IRS LoS channel matrix given as [NKDA15, NKC+19a]

$$[\mathbf{H}_1]_{m,n} = \exp\Big(j\frac{2\pi}{\lambda}\Big((m-1)d_{BS}\sin(\theta_{LoS_1}(n))\sin(\phi_{LoS_1}(n)) + (n-1)d_{IRS}\sin(\theta_{LoS_2}(n)) \times \sin(\phi_{LoS_2}(n))\Big)\Big), \tag{4.1}$$

where d_{BS} and d_{IRS} represent the distance between the BS antennas and the IRS elements respectively set as 0.5λ, $\theta_{LoS_1}(n)$ and $\phi_{LoS_1}(n)$, $n = 1 \ldots N$ are generated uniformly between 0 to π and 0 to 2π, respectively, while $\theta_{LoS_2}(n) = \pi - \theta_{LoS_1}(n)$ and $\phi_{LoS_2}(n) = \pi - \phi_{LoS_1}(n)$. The channel attenuation coefficients for the IRS-assisted channel and the direct channel are set as $\beta_{2,k}$ and $\beta_{d,k}$, respectively.

The considered multi-user setup is shown in Fig. 2 with K cell-edge users placed along an arc of radius 150m that spans angles from -30° to 30° with respect to the x-axis. Using (x, y, z) coordinates (in meters), the BS and IRS are deployed at $(0, 0, 25)$ and $(\bar{x}, \bar{y}, 40)$ respectively where $\bar{x}$ is the mean of x coordinates of all users and $\bar{y}$ is the mean of y coordinates of all users. Since the cell edge users have the most sensitive performance since they are more susceptible to blockages as well as high path losses, we will focus on the performance of these users. Additionally, we define $p_k = 1/K$, $\forall k$ and $P_{max} = 1$. The path loss for each link is calculated as $\beta = \frac{C_0}{d^\alpha}$, where C_0 is the fixed loss set as 30dB for all links and α is the path loss exponent set as 2 for $\mathbf{H}_1$, 2.8 for $\mathbf{h}_{2,k}$ and 3.5 for $\mathbf{h}_{d,k}$ as used in [WZ19b].

4.1 Deterministic Equivalent Validation

We will start with validating the tightness of the deterministic equivalence at large system dimension. For the purpose of this result, we let $\beta_{2,k} = c_k \beta_{d,k}$ and abstract $\frac{\beta_{2,k}}{\sigma^2}$ as ρ. Then, we plot in Fig. 4.2 against ρ, the sum-rate in (3.9) using the deterministic equivalent of the SINR in Theorem 3.1 as well as the Monte-Carlo simulated sum-rate in (2.23). The results are plotted against ρ for $M = K = N = 48$ and $\rho_{tr} = \{2, 8\}$dB.

From Fig. 4.2 we can see that the deterministic equivalent of the sum rate in (3.9) provides a tight approximation to the Monte-Carlo simulated sum-rate for moderate values of M, K, N. As expected, the sum-rate performance of the system deteriorates as ρ_{tr} decreases. Also, we observe that the approximation becomes less tight as ρ increases due to slower convergence to the deterministic equivalent. However, the match is still quite good for the entire range of ρ and therefore the deterministic equivalents derived in this thesis serve as useful tools to analytically study the performance of IRS-assisted systems.

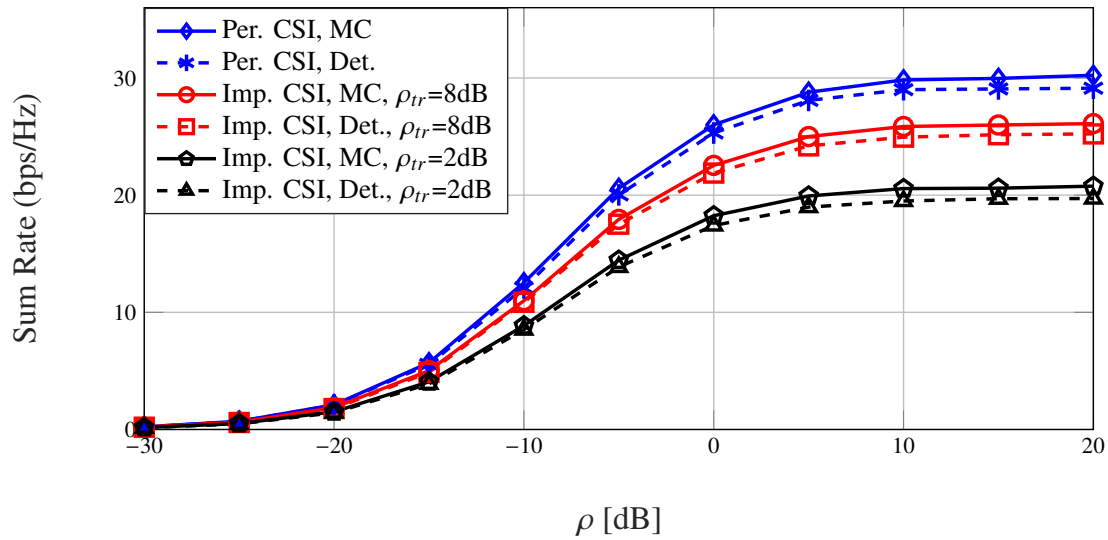

Figure 4.2: Numerical validation of the deterministic (det.) equivalent of the SINR against the Monte-Carlo (MC) values, under perfect (per.) and imperfect (imper.) CSI., where ρ is abstracted as $1/\sigma^2$.

4.2 IRS Performance with Respect to the Conventional System

In this section, we will compare the performance of an IRS-assisted system with conventional MISO systems along with providing useful insights on the required size of IRS to achieve similar performance as the conventional MISO system but at lower implementation cost.

4.2.1 Performance Comparison

We compare the performance of an IRS-assisted system with the conventional MISO system and showcase that for the scenario considered in Fig. 4.3, the IRS yields notable gain over the conventional system wherein the gains promised by large MISO systems can be obtained by using an IRS with many passive reflecting elements while using a smaller number of active antennas at the BS. In the following simulation results, we introduce the model for ρ_{tr} as $\rho_{tr} = \frac{p_c \tau_c}{\sigma^2}$, which depends on the noise variance σ^2 set as 10^{-17} Joules as well as the pilot Tx power p_c set as 1W and length of each of the $N+1$ channel estimation phases τ_s sec. The channel estimation period τ_c is defined as 0.01τ, where τ is the length of the coherence interval set as 10ms. Therefore $\tau_s = \frac{0.01\tau}{(N+1)}$. Note that for the conventional MIMO system where no IRS is deployed, we will have $\tau_s = 0.01\tau$. Under the block-fading channel model, the net achievable rate of user k in (2.6) is given

as $R_k = \left(1 - \frac{\tau_c}{\tau}\right) \log_2(1 + SINR_k)$. The net achievable sum-rate is then given as $R_{sum} = \sum_{k=1}^{K} R_k$. This is plotted in the subsequent figures.

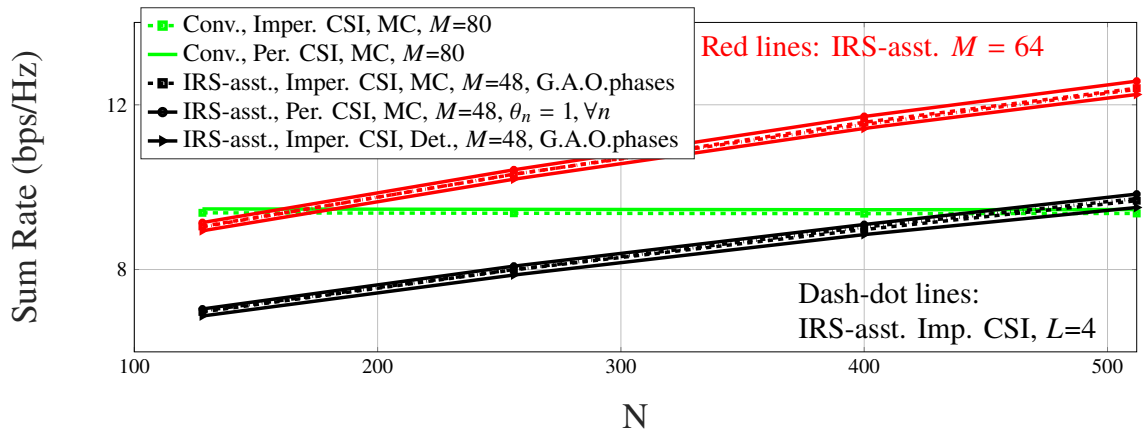

Figure 4.3: Sum-rate comparison of IRS-assisted (IRS-asst.) MISO system under gradient ascent algorithm optimized (G.A.O) phases and exhaustive search optimized phases, and comparison with sum-rate of conventional (conv.) MISO systems.

In Fig. 4.3, we show the effect of introducing an IRS on the sum-rate achieved by cell-edge users for varying number of BS antennas and IRS reflecting elements, i.e. $M = \{48, 64, 80\}$ and $N = \{128, 256, 400, 512\}$. We consider $K = 32$ users in the system and compare the performance with that of a conventional MISO systems with 80 active antennas at the BS. We plot IRS-assisted system sum rate while optimizing phase shifts using the gradient ascent algorithm proposed in Algorithm 1 (square marked curve), as well as using an exhaustive search (dot-dashed curve) over an L-dimension set $\mathcal{F}$ defined as $\mathcal{F} = 0, \triangle\theta, \ldots, \triangle\theta(L-1)$, where $\triangle\theta = \frac{2\pi}{L}$ and $L = 4$. Notice that the curves almost overlap with negligible difference, which depicts the minor effect of phase shift on the overall performance of an asymptotic IRS-assisted system. Additionally, with increasing number of IRS elements N, the IRS-assisted system outperforms the conventional large MISO system, by using a fewer number of active antennas at the BS. The result shows that the IRS-assisted system with 170 passive reflecting elements at the IRS and 64 active antennas at the BS can achieve the same performance as a conventional large MISO system with 80 active antennas. The same performance can also be achieved with $M = 48$ antennas using $N = 470$ reflecting elements at the IRS. Therefore, an IRS-assisted system can perform as well as a conventional large MIMO system with a reduced number of active antennas at the BS, making it an energy-efficient alternative

to technologies like Massive MIMO and network densification.

4.2.2 Impact of Channel Estimation Time

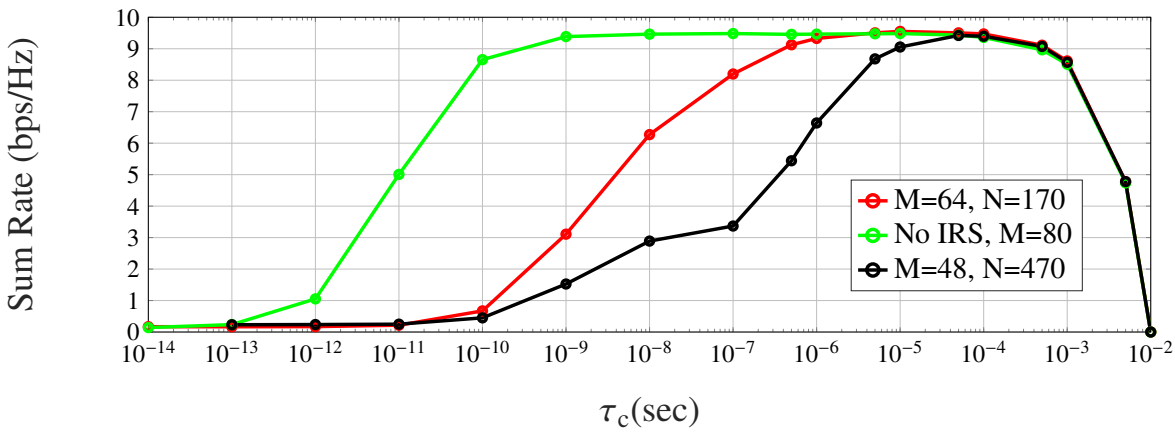

Figure 4.4: Sum-rate comparison of IRS-assisted (IRS-asst.) and conventional (conv.) MISO system under varying channel estimation time, where τ_c is the channel estimation time seconds.

We plot in Fig. 4.4 the net achievable rate against τ_c for a conventional MISO system (no IRS) with 80 active antennas at the BS serving $K = 32$ users. We also plot the net rates for IRS-assisted systems with a fewer number of active antennas at the BS. The value of N for each M is chosen to ensure that the IRS-assisted system performs as well as the conventional system that has 80 active antennas. We observe that the net rate is a unimodal function of τ_c. Specifically, $\tau_c = 10^{-4}$ is optimal for all the considered IRS-assisted MISO systems, whereas the conventional MISO system could perform as well at even lower value of τ_c. This shows that the performance of IRS-assisted systems is more sensitive to channel estimate quality as compared to conventional MISO systems, and that is due to the number of channels required to estimate in IRS-assisted system as compared to the conventional MISO system.

4.2.3 Impact of Channel Noise Under an IRS-Simplified Channel Model

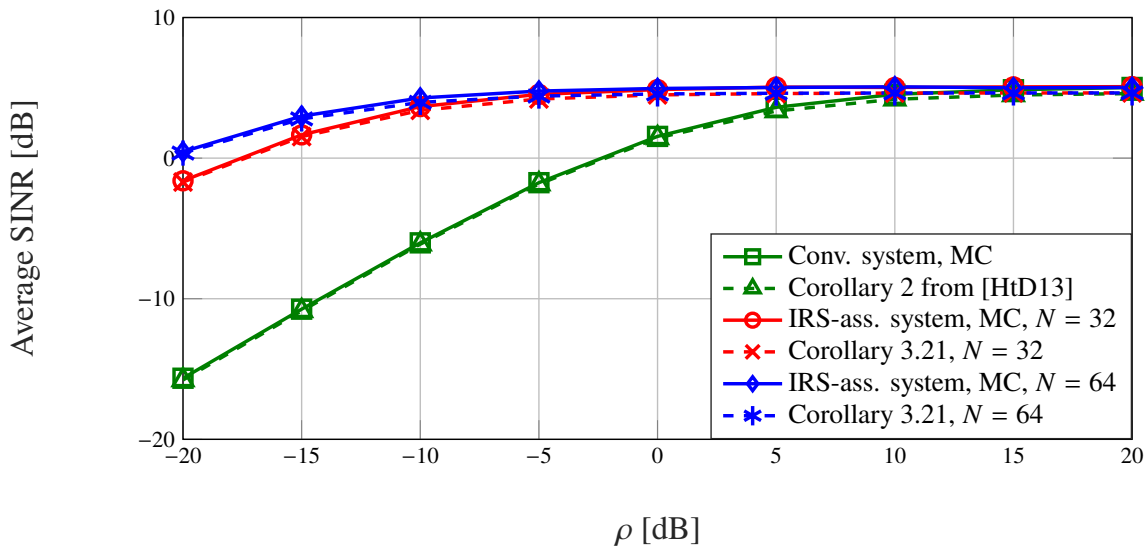

Figure 4.5: Performance of IRS-assisted system under the channel in (3.20), where ρ is abstracted as $1/\sigma^2$.

Fig. 4.5 studies the performance of IRS-assisted system against ρ under the simplified channel model in (3.20) for perfect CSI. The result in (3.21) in Corollary 3.21 is also plotted and the match between the Monte-Carlo simulated average SINR and the theoretical result is very good. As discussed in Sec. III-C, IRS is only beneficial under large system dimensions and Rayleigh fading when ρ takes small to moderate values, i.e. the system is noise-limited, which is often the case for cell edge users and users in dense urban-macro settings. For interference-limited scenarios (i.e. high ρ), the performance of IRS-assisted system approaches that of the conventional MISO system under Rayleigh fading. Note that the conventional MISO system was studied under the model in (3.20) in [HtD13].

4.2.4 Impact of Cell Radius

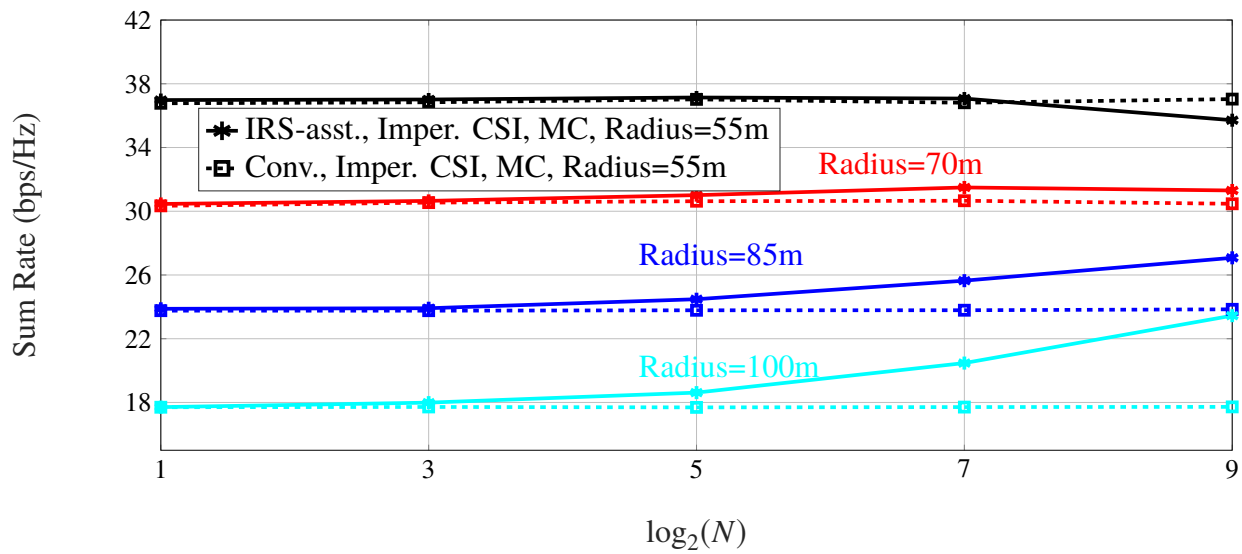

Figure 4.6: Performance analysis of IRS-assisted system under varying cell radius with $M = 50$ and $K = 32$

In Fig. 4.6 we depict the performance limit of IRS-assisted systems over varying cell radius. The curves are plotted for $M = 50$, $K = 32$ and under $N = [2^1, 2^3, 2^5, 2^7, 2^9]$. It is clear that an IRS in small cell radius, i.e. radius < 55 meters drops the system's performance while deploying IRS in larger cells, i.e 85 and 100 meters improves the signal received at the cell edge users. This observation can be explained as follows: In the case of small cell radius, the IRS-assisted system suffers a more dominant interference effect in the SINR value at the user's end as compared to the conventional MISO system. As the cell radius decreases, i.e. users become closer to BS, users will receive better intended symbol power from the direct channel than when receiving the signal from both the direct channel and IRS-assisted channel. For this reason, as shown in the black curves in Fig.4.6, we find that the conventional MISO systems for small cell edge users performs better than an IRS-assisted system. Nevertheless, towards larger cell radius, as shown in red and blue curves, the IRS-assisted system out-performs the conventional MISO system. This is clearly due to the large direct channel attenuation effect at the user's end, which is when the IRS array gain benefit would kick in. Deploying an IRS in such large cells will help the users leverage the gains that the IRS provides and improve the overall system's performance. For this reason we find

users in conventional MISO systems in small cells suffer from channel attenuation at a greater deal compared to users in IRS-assisted system.

4.3 Discussion

The IRS-assisted system was studied under a practical setting and compared to the conventional MISO system performance in terms of edge users' sum rate and number of BS active elements. IRS technology showed promising gains under large number of passive IRS elements while under relatively less active BS elements, thus providing cost efficient solution. The performance also showed sensitivity in the channel estimation time given the number of channels expected to estimate. IRS-assisted system performance limit was also investigated under varying cell radius and was shown that edge cell users receive stronger intended signal power under the conventional MISO system as compared to the IRS-assisted system in small cells. This proves that IRS-assisted systems are interference limited and are best deployed in large cells, where the high pathloss effect drops the performance of the direct channel and the IRS array gain benefit shows up. Finally, the derived SINR deterministic equivalence we proven to be tight in moderate system dimensions and a strong tool to use for system analysis.

Chapter 5

Conclusion and Future Direction

5.1 Conclusion

The IRS technology was proven to hold great potential in improving communication by effectively controlling the reflection of incident signals in favor of user reception, thus manipulating the propagation of radio waves in the environment and introducing a radically new way of communication. In this thesis work, we consider a MISO system in a Rayleigh fading environment with an IRS deployed to assist in communication. Specifically, we study a system with a BS consisting of M antennas communicating to K single antenna users via an IRS, which is equipped with N passive reflecting elements. We propose a novel MMSE based channel estimation protocol that considers the radio limitations in IRS technology. MMSE estimates for IRS-assisted channel and direct channels were derived under the estimation protocol and sum rate expressions under MRT precoding were formulated. Asymptotic performance was also considered in which the asymptotic equivalences of SINR and sum rate were obtained using RMT tools and insights on the impact of IRS phase shifts were provided. The derived asymptotic performance limit showed to yield an array gain but no beamforming gain. More specifically, IRS phases appear only in terms involving the estimation error of direct channel, which account for a negligible overall effect on performance. Our results also restrict the benefits achieved from an IRS assisted system under Rayleigh fading environment to interference limited scenarios. Our conclusions and derivations were supported by simulation results in Chapter 5.

5.1.1 Takeaways

With the above mentioned results, we can summarize the takeaways as follows:

- The derived asymptotic deterministic sum rate equivalences proved to be tight expressions even in moderate system dimension, and can be considered as useful tools in performance analysis and optimization.

- Asymptotic performance limit of an IRS-assisted system reveal that an IRS promises an array gain in a Rayleigh fading environment but loses on the beamforming gains. This was shown in both the derived asymptotic expressions and simulation results.

- IRS-assisted system performance is interference limited, were IRS's high sum rate gains appear to diminish in interference limited scenarios. This scenario can be shown in small cells, where the conventional MISO system appears to outperform an IRS-assisted MISO system for cell radius < 55m.

5.1.2 Limitations

The limitations of this work include the following:

- This work considers an ON-OFF channel estimation protocol that involves the $N + 1$ uplink sub-phases to obtain the final cascaded channel estimate for each user k. This obviously requires a good deal of training overhead to successfully estimate all channels for K users.

- This work considers MRT precoding for downlink transmission, which is not optimal when it comes to mitigating the interference effect in our proposed IRS-assisted MISO system.

To address the above limitations, the number of estimation sub-phases could perhaps be reduced, where the direct channel as well as IRS-assisted channels could be estimated in t sub-phases, such that $1 < t < N + 1$. This develops a trade-off between channel estimation accuracy and training overhead, but is worth investigating in case of limited resources. To address the interference drawback due to MRT precoding, we can consider zero forcing (ZF) or regularized zero forcing (RZF) precoders instead. The use of such precoders will show significant improvement in system's performance especially in scenarios where interference is high.

5.2 Future Direction

IRS technology is a relatively new technology proposed to improve multiuser communication systems. Therefore, the potential research directions are numerous and promising to consider. One direction which is now considered as an extension to this work, is studying the system's performance under correlated Rician environment and using Regularized zero forcing (RZF) precoder for transmit beamforming. This setting depicts a more practical scenario and the results are expected to show beamforming gain in the asymptotic limit given the line of sight (LOS) component of the Rician channel.

Another potential direction in IRS technology is integrating IRS in some current leading technologies including D2D communication as well as mmWave and THz communication. IRS is envisioned to enhance the individual data links by serving users dynamically and effectively manipulating signal reflection in favor of user reception.

Bibliography

[3Gp10] 3gpp, digital cellular telecommunications system (phase 2+); radio network planning aspects. *IEEE Systems Journal*, 2010. → pages 15

[AH16] H. B. Almelah and K. A. Hamdi. Spectral efficiency of distributed mimo systems with zf receivers. In *2016 IEEE Wireless Communications and Networking Conference*, pages 1–6, April 2016. → pages 2

[BCC+07] Ezio Biglieri, Robert Calderbank, Anthony Constantinides, Andrea Goldsmith, Arogyaswami Paulraj, and H. Vincent Poor. *Capacity limits of MIMO systems*, page 24–87. Cambridge University Press, 2007. → pages 4, 5

[BDRDR+19] Ertugrul Basar, Marco Di Renzo, Julien De Rosny, Merouane Debbah, Mohamed-Slim Alouini, and Rui Zhang. Wireless communications through reconfigurable intelligent surfaces. *IEEE Access*, 7:116753–116773, 2019. → pages 1

[BHS17] Emil Björnson, Jakob Hoydis, and Luca Sanguinetti. Massive mimo networks: Spectral, energy, and hardware efficiency. *Foundations and Trends® in Signal Processing*, 11(3-4):154–655, 2017. → pages 1

[BIK+16] S. Buzzi, C. I, T. E. Klein, H. V. Poor, C. Yang, and A. Zappone. A survey of energy-efficient techniques for 5g networks and challenges ahead. *IEEE Journal on Selected Areas in Communications*, 34(4):697–709, April 2016. → pages 17

[BMR17] Trevon Badloe, Jungho Mun, and Junsuk Rho. Metasurfaces-based absorption and reflection control: Perfect absorbers and reflectors. *Journal of Nanomaterials*, 2017:1–18, 11 2017. → pages 33

[BRdR+19] Ertugrul Basar, Marco Di Renzo, Julien de Rosny, Merouane Debbah, Mohamed-

Slim Alouini, and Rui Zhang. Wireless communications through reconfigurable intelligent surfaces, 2019. → pages 17

[BSHD15] E. Björnson, L. Sanguinetti, J. Hoydis, and M. Debbah. Optimal design of energy-efficient multi-user mimo systems: Is massive mimo the answer? *IEEE Transactions on Wireless Communications*, 14(6):3059–3075, June 2015. → pages 13, 14

[BSW+19] Emil Björnson, Luca Sanguinetti, Henk Wymeersch, Jakob Hoydis, and Thomas L. Marzetta. Massive mimo is a reality—what is next?: Five promising research directions for antenna arrays. *Digital Signal Processing*, 94:3 – 20, 2019. Special Issue on Source Localization in Massive MIMO. → pages 2, 4

[BV04] Stephen Boyd and Lieven Vandenberghe. *Convex Optimization*. Cambridge University Press, New York, NY, USA, 2004. → pages 42, 43

[CD11] Romain Couillet and Mérouane Debbah. *Random Matrix Methods for Wireless Communications*. Cambridge University Press, 2011. → pages 16, 34

[CLCY19] Jie Chen, Ying-Chang Liang, Hei Victor Cheng, and Wei Yu. Channel Estimation for Reconfigurable Intelligent Surface Aided Multi-User MIMO Systems. *arXiv e-prints*, page arXiv:1912.03619, Dec 2019. → pages 20, 21

[CSAJ19] Mostafa Zaman Chowdhury, Md. Shahjalal, Shakil Ahmed, and Yeong Min Jang. 6g wireless communication systems: Applications, requirements, technologies, challenges, and research directions, 2019. → pages 17

[EE16] Ariel Epstein and George V. Eleftheriades. Synthesis of passive lossless metasurfaces using auxiliary fields for reflectionless beam splitting and perfect reflection. *Phys. Rev. Lett.*, 117:256103, Dec 2016. → pages 33

[FHX+18] N. Fatema, G. Hua, Y. Xiang, D. Peng, and I. Natgunanathan. Massive mimo linear precoding: A survey. *IEEE Systems Journal*, 12(4):3920–3931, Dec 2018. → pages 13, 14

[GKH+07] David Gesbert, Marios Kountouris, Robert W. Heath, Chan byoung Chae, and Thomas Sälzer. From single user to multiuser communications: Shifting the mimo paradigm. In *IEEE Sig. Proc. Magazine*, 2007. → pages 2, 7

[GLCL19] Huayan Guo, Ying-Chang Liang, Jie Chen, and Erik G. Larsson. Weighted sum-rate optimization for intelligent reflecting surface enhanced wireless networks, 2019. → pages 20

[Gol05] Andrea Goldsmith. *Wireless Communications*. Cambridge University Press, USA, 2005. → pages 3, 4, 9

[HtD13] J. Hoydis, S. ten Brink, and M. Debbah. Massive mimo in the ul/dl of cellular networks: How many antennas do we need? *IEEE Journal on Selected Areas in Communications*, 31(2):160–171, February 2013. → pages 27, 31, 33, 39, 40, 50

[HY19] Z. He and X. Yuan. Cascaded channel estimation for large intelligent metasurface assisted massive MIMO. *IEEE Wireless Communications Letters*, pages 1–1, 2019. → pages 20, 21

[HY20] Z. He and X. Yuan. Cascaded channel estimation for large intelligent metasurface assisted massive mimo. *IEEE Wireless Communications Letters*, 9(2):210–214, Feb 2020. → pages 26

[JC19] Tobias Lindstrøm Jensen and Elisabeth De Carvalho. An optimal channel estimation scheme for intelligent reflecting surfaces based on a minimum variance unbiased estimator, 2019. → pages 27

[JKL+17] Hyoungju Ji, Younsun Kim, Juho Lee, Eko Onggosanusi, Younghan Nam, Jianzhong Zhang, Byungju Lee, and Byonghyo Shim. Overview of full-dimension mimo in lte-advanced pro. *IEEE Communications Magazine*, 55(2):176–184, Feb 2017. → pages 3

[Kay97] S. M. Kay. *Fundamentals of Statistical Signal Processing: Estimation Theory*. Prentice Hall, 1997. → pages 11

[KUV19] A. K. Kocharlakota, K. Upadhya, and S. A. Vorobyov. On the spectral efficiency for massive mimo systems with imperfect spacial covariance information, 2019. → pages 2

[LD19] Tobias Lindstrøm Jensen and Elisabeth De Carvalho. An Optimal Channel Estimation Scheme for Intelligent Reflecting Surfaces based on a Minimum Variance Unbiased Estimator. *arXiv e-prints*, page arXiv:1909.09440, Sep 2019. → pages 20

[LDY+19] Sixian Li, Bin Duo, Xiaojun Yuan, Ying-Chang Liang, and Marco Di Renzo. Reconfigurable intelligent surface assisted uav communication: Joint trajectory design and passive beamforming, 2019. → pages 20

[LETM14] E. G. Larsson, O. Edfors, F. Tufvesson, and T. L. Marzetta. Massive mimo for next generation wireless systems. *IEEE Communications Magazine*, 52(2):186–195, February 2014. → pages 10

[LLS+14] L. Lu, G. Y. Li, A. L. Swindlehurst, A. Ashikhmin, and R. Zhang. An overview of massive mimo: Benefits and challenges. *IEEE Journal of Selected Topics in Signal Processing*, 8(5):742–758, Oct 2014. → pages 5

[Mar06] T. L. Marzetta. How much training is required for multiuser mimo? In *2006 Fortieth Asilomar Conference on Signals, Systems and Computers*, pages 359–363, Oct 2006. → pages 9

[Mar10] T. L. Marzetta. Noncooperative cellular wireless with unlimited numbers of base station antennas. *IEEE Transactions on Wireless Communications*, 9(11):3590–3600, November 2010. → pages 12

[Mar15] T. L. Marzetta. Massive mimo: An introduction. *Bell Labs Technical Journal*, 20:11–22, 2015. → pages 1, 5, 7

[MBB+00] Aris L. Moustakas, Harold U. Baranger, Leon Balents, Anirvan M. Sengupta, and Steven H. Simon. Communication through a diffusive medium: Coherence and capacity. *Science*, 287(5451):287–290, 2000. → pages 15

[Med00] M. Medard. The effect upon channel capacity in wireless communications of perfect and imperfect knowledge of the channel. *IEEE Transactions on Information Theory*, 46(3):933–946, May 2000. → pages 31

[MIA16] D. Muirhead, M. A. Imran, and K. Arshad. A survey of the challenges, opportunities and use of multiple antennas in current and future 5g small cell base stations. *IEEE Access*, 4:2952–2964, 2016. → pages 17

[MJ19a] D. Mishra and H. Johansson. Channel estimation and low-complexity beamforming design for passive intelligent surface assisted miso wireless energy transfer. In *ICASSP 2019 - 2019 IEEE International Conference on Acoustics, Speech and Signal Processing (ICASSP)*, pages 4659–4663, May 2019. → pages 11

[MJ19b] D. Mishra and H. Johansson. Channel estimation and low-complexity beamforming design for passive intelligent surface assisted MISO wireless energy transfer. In *2019 IEEE International Conference on Acoustics, Speech and Signal Processing (ICASSP)*, pages 4659–4663, May 2019. → pages 20

[MLG+19] Xidong Mu, Yuanwei Liu, Li Guo, Jiaru Lin, and Naofal Al-Dhahir. Exploiting intelligent reflecting surfaces in multi-antenna aided noma systems, 2019. → pages 20, 33

[MLYN16] Thomas L. Marzetta, Erik G. Larsson, Hong Yang, and Hien Quoc Ngo. *Fundamentals of Massive MIMO*. Cambridge University Press, 2016. → pages 2, 3, 5, 15

[MSI17] E. Mukubwa, O. A. Sokoya, and D. S. Ilcev. Comparison and analysis of massive mimo linear precoding schemes in the downlink. In *2017 IEEE AFRICON*, pages 187–191, Sep. 2017. → pages 11

[Ngo15] Hien Quoc Ngo. Massive mimo: Fundamentals and system designs. 2015. → pages 1, 2, 9, 14

[NKC+19a] Qurrat-Ul-Ain Nadeem, Abla Kammoun, Anas Chaaban, Mérouane Debbah, and

Mohamed-Slim Alouini. Asymptotic analysis of large intelligent surface assisted MIMO communication. *CoRR*, abs/1903.08127, 2019. → pages 45

[NKC+19b] Qurrat-Ul-Ain Nadeem, Abla Kammoun, Anas Chaaban, Merouane Debbah, and Mohamed-Slim Alouini. Asymptotic max-min sinr analysis of reconfigurable intelligent surface assisted miso systems, 2019. → pages 20, 33

[NKDA15] Q. Nadeem, A. Kammoun, M. Debbah, and M. Alouini. A generalized spatial correlation model for 3d mimo channels based on the fourier coefficients of power spectrums. *IEEE Transactions on Signal Processing*, 63(14):3671–3686, July 2015. → pages 45

[NKDA19] Q. Nadeem, A. Kammoun, M. Debbah, and M. Alouini. Asymptotic analysis of rzf over double scattering channels with mmse estimation. *IEEE Transactions on Wireless Communications*, 18(5):2509–2526, May 2019. → pages 31, 33

[NLM13] H. Q. Ngo, E. G. Larsson, and T. L. Marzetta. Energy and spectral efficiency of very large multiuser mimo systems. *IEEE Transactions on Communications*, 61(4):1436–1449, April 2013. → pages 5

[Ren19] Debbah M. Phan-Huy D. et al. Renzo, M.D. Smart radio environments empowered by reconfigurable ai meta-surfaces: an idea whose time has come. *CoRR*, abs/0906.3682, 2019. → pages 17, 18

[RPL+13] F. Rusek, D. Persson, B. K. Lau, E. G. Larsson, T. L. Marzetta, O. Edfors, and F. Tufvesson. Scaling up mimo: Opportunities and challenges with very large arrays. *IEEE Signal Processing Magazine*, 30(1):40–60, Jan 2013. → pages 1, 5, 10, 12, 16

[TAA19a] Abdelrahman Taha, Muhammad Alrabeiah, and Ahmed Alkhateeb. Enabling large intelligent surfaces with compressive sensing and deep learning, 2019. → pages 26

[TAA19b] Abdelrahman Taha, Muhammad Alrabeiah, and Ahmed Alkhateeb. Enabling large intelligent surfaces with compressive sensing and deep learning, 2019. → pages 33

[TSJP16] X. Tan, Z. Sun, J. M. Jornet, and D. Pados. Increasing indoor spectrum sharing capacity using smart reflect-array. In *2016 IEEE International Conference on Communications (ICC)*, pages 1–6, May 2016. → pages 20

[TSKJ18] X. Tan, Z. Sun, D. Koutsonikolas, and J. M. Jornet. Enabling indoor mobile millimeter-wave networks based on smart reflect-arrays. In *IEEE INFOCOM 2018 - IEEE Conference on Computer Communications*, pages 270–278, April 2018. → pages 20

[TV04] Antonio M. Tulino and Sergio Verdú. Random matrix theory and wireless communications. *Commun. Inf. Theory*, 1(1):1–182, June 2004. → pages 16, 34

[TV05] David Tse and Pramod Viswanath. *Fundamentals of Wireless Communication*. Cambridge University Press, USA, 2005. → pages 3, 5, 7, 8, 9

[VT03] P. Viswanath and D. N. C. Tse. Sum capacity of the vector gaussian broadcast channel and uplink-downlink duality. *IEEE Transactions on Information Theory*, 49(8):1912–1921, 2003. → pages 6

[WCDS12a] S. Wagner, R. Couillet, M. Debbah, and D. T. M. Slock. Large system analysis of linear precoding in correlated miso broadcast channels under limited feedback. *IEEE Transactions on Information Theory*, 58(7):4509–4537, July 2012. → pages 8, 11, 33

[WCDS12b] Sebastian Wagner, Romain Couillet, Mérouane Debbah, and Dirk T. M. Slock. Large system analysis of linear precoding in correlated miso broadcast channels under limited feedback. *IEEE Transactions on Information Theory*, 58(7):4509–4537, Jul 2012. → pages 16

[WLC+17] Q. Wu, G. Y. Li, W. Chen, D. W. K. Ng, and R. Schober. An overview of sustainable green 5g networks. *IEEE Wireless Communications*, 24(4):72–80, Aug 2017. → pages 17

[WZ18] Qingqing Wu and Rui Zhang. Intelligent reflecting surface enhanced wireless network via joint active and passive beamforming, 2018. → pages 20, 33

[WZ19a] Q. Wu and R. Zhang. Beamforming optimization for intelligent reflecting surface with discrete phase shifts. In *ICASSP 2019 - 2019 IEEE International Conference on Acoustics, Speech and Signal Processing (ICASSP)*, pages 7830–7833, May 2019. → pages 20

[WZ19b] Q. Wu and R. Zhang. Intelligent reflecting surface enhanced wireless network via joint active and passive beamforming. *IEEE Transactions on Wireless Communications*, 18(11):5394–5409, Nov 2019. → pages 20, 46

[WZ19c] Q. Wu and R. Zhang. Towards smart and reconfigurable environment: Intelligent reflecting surface aided wireless network. *IEEE Communications Magazine*, pages 1–7, 2019. → pages 18

[WZ19d] Qingqing Wu and Rui Zhang. Beamforming optimization for wireless network aided by intelligent reflecting surface with discrete phase shifts, 2019. → pages 20

[YXXL19] P. Yang, Y. Xiao, M. Xiao, and S. Li. 6g wireless communications: Vision and potential techniques. *IEEE Network*, 33(4):70–75, July 2019. → pages 17

[YZZ19a] Changsheng You, Beixiong Zheng, and Rui Zhang. Intelligent Reflecting Surface with Discrete Phase Shifts: Channel Estimation and Passive Beamforming. *arXiv e-prints*, page arXiv:1911.03916, November 2019. → pages 20

[YZZ19b] Changsheng You, Beixiong Zheng, and Rui Zhang. Intelligent reflecting surface with discrete phase shifts: Channel estimation and passive beamforming, 2019. → pages 27

[ZBM+19] Jiayi Zhang, Emil Björnson, Michail Matthaiou, Derrick Wing Kwan Ng, Hong Yang, and David J. Love. Multiple antenna technologies for beyond 5g, 2019. → pages 18

Appendix A

Proof of the Channel Correlation

A.1 Proof of (2.2)

To compute $\mathbf{A}_k$ we use the definition $\mathbf{h}_k = \mathbf{h}_{d,k} + \sum_{i=1}^{N} \mathbf{h}_{0,i,k}\theta_i$ and $\mathbf{h}_{0,i,k} = \mathbf{H}_1(:,i)\mathbf{h}_{2,k}(i)$, where $\mathbf{H}_1(: .i)$ is the i'th column of $\mathbf{H}_1$ matrix, to obtain,

$$\mathbf{A}_k = \mathbb{E}[\mathbf{h}_k\mathbf{h}_k^H] = \mathbb{E}[(\mathbf{h}_{d,k} + \sum_{i=1}^{N} \mathbf{h}_{0,i,k}v_i)(\mathbf{h}_{d,k}^H + \sum_{j=1}^{N} \theta_i^*\mathbf{h}_{0,i,k}^H)], \tag{A.1}$$

$$= \mathbb{E}[\mathbf{h}_{d,k}\mathbf{h}_{d,k}^H] + \mathbb{E}[\sum_{i=1}^{N}\sum_{j=1}^{N} \mathbf{h}_{0,i,k}\theta_i\theta_j^*\mathbf{h}_{0,j,k}^H], \tag{A.2}$$

$$= \mathbb{E}[\mathbf{h}_{d,k}\mathbf{h}_{d,k}^H] + \sum_{i=1}^{N}\sum_{j=1}^{N} \mathbf{H}_1(:,i)\theta_i\mathbb{E}[\mathbf{h}_{2,k}(i)\mathbf{h}_{2,k}^H(j)]\theta_j^*\mathbf{H}_1(:,j)^H. \tag{A.3}$$

Due to independence of $\mathbf{h}_{2,k}(i)$ and $\mathbf{h}_{2,k}(j)$ for $i \neq j$ the above expression can be reduced to,

$$A_k = \beta_{d,k}\mathbf{I}_M + \beta_{2,k}\sum_{i=1}^{N} \mathbf{H}_1(:,i)\theta_i\theta_i^*\mathbf{H}_1(:,i)^H. \tag{A.4}$$

Representing (A.4) in a matrix form, we obtain,

$$A_k = \beta_{d,k}\mathbf{I}_M + \beta_{2,k}\mathbf{H}_1\Theta\Theta^H\mathbf{H}_1^H \tag{A.5}$$

as given in (2.2).

A.2 Proof of (2.13)

Given the observed training signal, $\mathbf{r}_{1,k}^{tr}$, in the first sub-interval of the channel estimation phase given in (2.12), we can write the MMSE estimate of $\hat{\mathbf{h}}_{d,k}$ as

$$\hat{\mathbf{h}}_{d,k} = \mathbf{A}\mathbf{r}_{1,k}^{tr}, \tag{A.6}$$

where $\mathbf{A}$ is found as the solution to $\min_{\mathbf{A}} E[|\hat{\mathbf{h}}_{d,k} - \mathbf{h}_{d,k}|^2]$ and turns out to be $\mathbf{A} = \mathbb{E}[\mathbf{r}^{tr}_{1,k}\mathbf{h}^H_{d,k}](\mathbb{E}[\mathbf{r}^{tr}_{1,k}\mathbf{r}^{trH}_{1,k}])^{-1}$.

We now compute $\mathbb{E}[\mathbf{r}^{tr}_{1,k}\mathbf{h}^H_{d,k}]$ by noting that $\mathbf{n}_{i,k}$ and $\mathbf{h}_{d,k}$ are independent random vectors, to obtain,

$$\mathbb{E}[\mathbf{r}^{tr}_{1,k}\mathbf{h}^H_{d,k}] = \mathbb{E}[(\mathbf{h}_{d,k} + \mathbf{n}_{1,k})\mathbf{h}^H_{d,k}], \tag{A.7}$$

$$= \mathbb{E}[(\mathbf{h}_{d,k}\mathbf{h}^H_{d,k} + \mathbf{h}^H_{d,k}\mathbf{n}_{1,k})] \tag{A.8}$$

$$= \mathbb{E}[\mathbf{h}_{d,k}\mathbf{h}^H_{d,k}] = \beta_{d,k}\mathbf{I}_M. \tag{A.9}$$

Next we find $\mathbb{E}[\mathbf{r}^{tr}_{1,k}\mathbf{r}^{trH}_{1,k}]$ as,

$$\mathbb{E}[\mathbf{r}^{tr}_{1,k}\mathbf{r}^{trH}_{1,k}] = \mathbb{E}[(\mathbf{h}_{d,k} + \mathbf{n}_{1,k})(\mathbf{h}_{d,k} + \mathbf{n}_{1,k}), \tag{A.10}$$

$$= \mathbb{E}[\mathbf{h}_{d,k}\mathbf{h}_{d,k}] + \mathbb{E}[\mathbf{n}_{1,k}\mathbf{n}^H_{1,k}], \tag{A.11}$$

$$= \beta_{d,k}\mathbf{I}_M + \frac{1}{\rho_{tr}}\mathbf{I}_M. \tag{A.12}$$

Putting these expression together, we obtain,

$$\hat{\mathbf{h}}_{d,k} = \beta_{d,k}\mathbf{I}_M\left(\beta_{d,k}\mathbf{I}_M + \frac{1}{\rho_{tr}}\mathbf{I}_M\right)^{-1}\mathbf{r}^{tr}_{1,k} \tag{A.13}$$

which confirms (2.13)

A.3 Proof of (2.16)

The MMSE estimate of $\mathbf{h}_{0,i,k}$ is obtained as,

$$\hat{\mathbf{h}}_{0,i,k} = \mathbf{A}\tilde{\mathbf{r}}^{tr}_{i,k} \tag{A.14}$$

where $\mathbf{A} = E[\tilde{\mathbf{r}}^{tr}_{i,k}\mathbf{h}^H_{0,i,k}](E[\tilde{\mathbf{r}}^{tr}_{i,k}\tilde{\mathbf{r}}^{trH}_{i,k}])^{-1}$ and $\tilde{\mathbf{r}}^{tr}_{i,k}$ is given in (2.15). We first find the expression of $E[\tilde{\mathbf{r}}^{tr}_{i,k}\mathbf{h}^H_{0,i,k}]$ by noting that that $\mathbf{n}_{i,k}$ and $\mathbf{h}_{0,i,k}$ are independent random vectors, and $\tilde{\mathbf{h}}_{d,k}$ and $\mathbf{h}^H_{0,i,k}$ are independent random vectors. Therefore,

$$\mathbb{E}[\tilde{\mathbf{r}}^{tr}_{i,k}\mathbf{h}^H_{0,i,k}] = \mathbb{E}[(\tilde{\mathbf{h}}_{d,k} + \mathbf{h}_{0,i,k} + \mathbf{n}_{i,k})\mathbf{h}^H_{o,i,k}] \tag{A.15}$$

$$= \mathbb{E}[(\tilde{\mathbf{h}}_{d,k}\mathbf{h}^H_{0,i,k} + \mathbf{h}_{0,i,k}\mathbf{h}^H_{0,i,k} + \mathbf{h}^H_{0,i,k}\mathbf{n}_{i,k})], \tag{A.16}$$

$$= \mathbb{E}[\mathbf{h}_{0,i,k}\mathbf{h}^H_{0,i,k}] = \beta_{2,k}\mathbf{H}_1(:,i)\mathbf{H}_1(:,i)^H. \tag{A.17}$$

Next we find $E[\tilde{\mathbf{r}}_{i,k}^{tr}\tilde{\mathbf{r}}_{i,k}^{trH}]$ by using the independence of the following pair of vectors ($\mathbf{n}_{i,k}$, $\mathbf{h}_{0,i,k}$) and ($\tilde{\mathbf{h}}_{d,k}$,$\mathbf{h}_{0,i,k}^{H}$), to obtain,

$$\mathbb{E}[\tilde{\mathbf{r}}_{i,k}^{tr}\tilde{\mathbf{r}}_{i,k}^{trH}] = \mathbb{E}[(\tilde{\mathbf{h}}_{d,k} + \mathbf{h}_{0,i,k} + \mathbf{n}_{i,k})(\tilde{\mathbf{h}}_{d,k} + \mathbf{h}_{0,i,k} + \mathbf{n}_{i,k})^{H}], \tag{A.18}$$

$$= \mathbb{E}[\tilde{\mathbf{h}}_{d,k}\tilde{\mathbf{h}}_{d,k}] + \mathbb{E}[\mathbf{h}_{0,i,k}\mathbf{h}_{0,i,k}^{H}] + E[\mathbf{n}_{i,k}\mathbf{n}_{i,k}^{H}], \tag{A.19}$$

$$= \mathbf{C}_{\tilde{\mathbf{h}}_{d,k}\tilde{\mathbf{h}}_{d,k}^{H}} + \beta_{2,k}\mathbf{H}_1(:,i)\mathbf{H}_1(:,i)^{H} + \frac{1}{\rho_{tr}}\mathbf{I}_M. \tag{A.20}$$

To obtain $\mathbf{C}_{\tilde{\mathbf{h}}_{d,k}\tilde{\mathbf{h}}_{d,k}}^{H}$, we recall that $\tilde{\mathbf{h}}_{d,k} = \mathbf{h}_{d,k} - \hat{\mathbf{h}}_{d,k}$ and therefore,

$$\mathbf{C}_{\tilde{\mathbf{h}}_{d,k}\tilde{\mathbf{h}}_{d,k}^{H}} = \mathbb{E}[\tilde{\mathbf{h}}_{d,k}\tilde{\mathbf{h}}_{d,k}^{H}] = \mathbb{E}[\mathbf{h}_{d,k}\mathbf{h}_{d,k}^{H}] - \mathbb{E}[\hat{\mathbf{h}}_{d,k}\hat{\mathbf{h}}_{d,k}^{H}], \tag{A.21}$$

$$= \beta_{d,k}\mathbf{I}_M + \mathbb{E}[\mathbf{R}_{d,k}\mathbf{Q}_{d,k}(\mathbf{h}_{d,k} + \mathbf{n}_{1,k})(\mathbf{h}_{d,k}^{H} + \mathbf{n}_{1,k}^{H})\mathbf{Q}_{d,k}^{H}\mathbf{R}_{d,k}^{H}]. \tag{A.22}$$

Note that $\mathbf{h}_{d,k}$ and $\mathbf{n}_{1,k}$ are independent random vectors and therefore,

$$\begin{aligned}\mathbf{C}_{\tilde{\mathbf{h}}_{d,k}\tilde{\mathbf{h}}_{d,k}^{H}} &= \beta_{d,k}\mathbf{I}_M + \mathbf{R}_{d,k}\mathbf{Q}_{d,k}\mathbb{E}[\mathbf{h}_{d,k}\mathbf{h}_{d,k}^{H}]\mathbf{Q}_{d,k}^{H}\mathbf{R}_{d,k}^{H} + \\ &\qquad \mathbf{R}_{d,k}\mathbf{Q}_{d,k}\mathbb{E}[\mathbf{n}_{1,k}\mathbf{n}_{1,k}^{H}]\mathbf{Q}_{d,k}^{H}\mathbf{R}_{d,k}^{H},\end{aligned} \tag{A.23}$$

$$= \beta_{d,k}\mathbf{I}_M + \beta_{d,k}\mathbf{R}_{d,k}\mathbf{Q}_{d,k}\mathbf{Q}_{d,k}^{H}\mathbf{R}_{d,k}^{H} + \frac{1}{\rho_{tr}}\mathbf{R}_{d,k}\mathbf{Q}_{d,k}\mathbf{Q}_{d,k}^{H}\mathbf{R}_{d,k}^{H}, \tag{A.24}$$

$$= \beta_{d,k}\mathbf{I}_M + \mathbf{R}_{d,k}\mathbf{Q}_{d,k}\mathbf{R}_{d,k}. \tag{A.25}$$

Therefore, putting (A.25) back in (A.20) and using it along with (A.17) in (A.14) we obtain,

$$\begin{aligned}\hat{\mathbf{h}}_{0,i,k} &= \beta_{2,k}\mathbf{H}_1(:,i)\mathbf{H}_1(:,i)^{H} \\ &\quad \left(\mathbf{C}_{\tilde{\mathbf{h}}_{d,k}\tilde{\mathbf{h}}_{d,k}^{H}} + \beta_{2,k}\mathbf{H}_1(:,i)\mathbf{H}_1(:,i)^{H} + \frac{1}{\rho_{tr}}\mathbf{I}_M\right)^{-1}\tilde{\mathbf{r}}_{i,k}^{tr}\end{aligned} \tag{A.26}$$

as given in (2.16).

A.4 Proof of (2.17)

Recall $\hat{\mathbf{h}}_k = \hat{\mathbf{h}_{d,k}} + \sum_{i=1}^{N}\hat{\mathbf{h}}_{0,i,k}\theta_i$ and that $\hat{\mathbf{h}}_{0,i,k}$ and $\hat{\mathbf{h}}_{d,k}$ are independent, therefore:

$$\mathbb{E}[\hat{\mathbf{h}}_k\hat{\mathbf{h}}_k^{H}] = \mathbb{E}[(\hat{\mathbf{h}_{d,k}} + \sum_{i=1}^{N}\hat{\mathbf{h}}_{0,i,k}\theta_i)(\hat{\mathbf{h}_{d,k}} + \sum_{j=1}^{N}\hat{\mathbf{h}}_{0,j,k}\theta_j)^{*}], \tag{A.27}$$

$$= \mathbb{E}[\hat{\mathbf{h}}_{d,k}\hat{\mathbf{h}}_{d,k}^{H}] + \sum_{j=1}^{N}\sum_{i=1}^{N}\theta_i E[\hat{\mathbf{h}}_{0,i,k}\hat{\mathbf{h}}_{0,j,k}^{H}]\theta_j^{*}, \tag{A.28}$$

where $\mathbb{E}[\hat{\mathbf{h}}_{d,k}\hat{\mathbf{h}}_{d,k}^H] = \mathbf{R}_{d,k}\mathbf{Q}_{d,k}\mathbf{R}_{d,k}$.

We now compute $\sum_{j=1}^{N}\sum_{i=1}^{N}\theta_i\mathbb{E}[\hat{\mathbf{h}}_{0,i,k}\hat{\mathbf{h}}_{0,j,k}^H]\theta_j^*$ as,

$$\begin{aligned}
&\sum_{j=1}^{N}\sum_{i=1}^{N}\theta_i\mathbb{E}[\hat{\mathbf{h}}_{0,i,k}\hat{\mathbf{h}}_{0,j,k}^H]\theta_j^* \\
&= \sum_{j=1}^{N}\sum_{i=1}^{N}\theta_i\mathbb{E}[\mathbf{R}_{0,i,k}\mathbf{Q}_{i,k}(\tilde{\mathbf{h}}_{d,k} + \mathbf{h}_{0,i,k} + \mathbf{n}_{i,k}) \\
&\qquad\qquad (\tilde{\mathbf{h}}_{d,k}^H + \mathbf{h}_{0,j,k}^H + \mathbf{n}_{j,k}^H)\mathbf{Q}_{j,k}^H\mathbf{R}_{0,j,k}]\theta_j^*, \\
&= \sum_{j=1}^{N}\sum_{i=1}^{N}\theta_i(\mathbf{R}_{0,i,k}\mathbf{Q}_{i,k}\mathbb{E}[\tilde{\mathbf{h}}_{d,k}\tilde{\mathbf{h}}_{d,k}]\mathbf{Q}_{j,k}^H\mathbf{R}_{0,j,k}^H + \\
&\qquad \mathbf{R}_{0,i,k}\mathbf{Q}_{i,k}\mathbb{E}[\mathbf{h}_{0,i,k}\mathbf{h}_{0,i,k}]\mathbf{Q}_{j,k}^H\mathbf{R}_{0,j,k}^H + \\
&\qquad \mathbf{R}_{0,i,k}\mathbf{Q}_{i,k}E[\mathbf{n}_{i,k}\mathbf{n}_{i,k}^H]\mathbf{Q}_{j,k}^H\mathbf{R}_{0,j,k}^H)\theta_j^*.
\end{aligned} \tag{A.29}$$

Considering the independence between $\tilde{\mathbf{h}}_{d,k}$, $\mathbf{h}_{0,i,k}$ and $\mathbf{n}_{i,k}$

$$\begin{aligned}
\sum_{j=1}^{N}\sum_{i=1}^{N}\theta_i\mathbb{E}[\hat{\mathbf{h}}_{0,i,k}\hat{\mathbf{h}}_{0,j,k}^H]\theta_j^* &= \sum_{j=1}^{N}\sum_{i=1}^{N}\theta_i\mathbf{R}_{0,i,k}\mathbf{Q}_{i,k}\mathbf{C}_{\tilde{\mathbf{h}}_{d,k}\tilde{\mathbf{h}}_{d,k}}\mathbf{Q}_{j,k}^H\mathbf{R}_{0,j,k}^H\theta_j^* \\
&\quad + \sum_{i=1}^{N}\mathbf{R}_{0,i,k}\mathbf{Q}_{i,k}\mathbf{R}_{0,i,k}\mathbf{Q}_{i,k}^H\mathbf{R}_{0,i,k}^H \\
&\quad + \sum_{i=1}^{N}\mathbf{R}_{0,i,k}\mathbf{Q}_{i,k}\frac{1}{\rho_{tr}}\mathbf{I}_M\mathbf{Q}_{i,k}^H\mathbf{R}_{0,i,k}^H
\end{aligned} \tag{A.30}$$

The expression can be simplified to obtain,

$$\begin{aligned}
\sum_{j=1}^{N}\sum_{i=1}^{N}\theta_iE[\hat{\mathbf{h}}_{0,i,k}\hat{\mathbf{h}}_{0,j,k}^H]\theta_j^* &= \sum_{j=1}^{N}\sum_{i=1}^{N}\theta_i\mathbf{R}_{0,i,k}\mathbf{Q}_{i,k}\mathbf{C}_{\tilde{\mathbf{h}}_{d,k}\tilde{\mathbf{h}}_{d,k}}\mathbf{Q}_{j,k}^H\mathbf{R}_{0,j,k}^H\theta_j^* \\
&\quad + \sum_{i=1}^{N}\mathbf{R}_{0,i,k}\mathbf{Q}_{i,k}(\mathbf{R}_{0,i,k} + \frac{1}{\rho_{tr}}\mathbf{I}_M)\mathbf{Q}_{i,k}^H\mathbf{R}_{0,i,k}^H
\end{aligned} \tag{A.31}$$

Therefore,

$$\begin{aligned}
E[\hat{\mathbf{h}}_k\hat{\mathbf{h}}_k^H] = \mathbf{R}_{d,k}\mathbf{Q}_{d,k}\mathbf{R}_{d,k} &+ \sum_{j=1}^{N}\sum_{i=1}^{N}\theta_i\mathbf{R}_{0,i,k}\mathbf{Q}_{i,k}\mathbf{C}_{\tilde{\mathbf{h}}_{d,k}\tilde{\mathbf{h}}_{d,k}}\mathbf{Q}_{j,k}^H\mathbf{R}_{0,j,k}^H\theta_j^* + \\
&\sum_{i=1}^{N}\mathbf{R}_{0,i,k}\mathbf{Q}_{i,k}(\mathbf{R}_{0,i,k} + \frac{1}{\rho_{tr}}\mathbf{I}_M)\mathbf{Q}_{i,k}^H\mathbf{R}_{0,i,k}^H
\end{aligned} \tag{A.32}$$

as in (2.17).

Appendix B

Proof of Theorem 3.1

In this section we derive the deterministic equivalence of SINR under the MRT precoding. The strategy is to look at the SINR expression in (2.22) as consisting of three separate terms: 1) the scaled signal power $\frac{p_k}{K}|\mathbf{h}_k^H\hat{\mathbf{h}}_k|^2$, 2) the scaled interference power $\sum_{l\neq k}\frac{p_l}{K}|\mathbf{h}_k^H\hat{\mathbf{h}}_l|^2$, and 3) the power normalization term Ψ. We will derive the deterministic equivalent for each of these terms separately and then obtain the final expression $\gamma^{\circ}_{k,MRT}$.

Deterministic equivalence for $\frac{1}{K}\boldsymbol{h}_k^H\hat{\boldsymbol{h}}_k$:

We have,

$$\frac{1}{K}\mathbf{h}_k^H\hat{\mathbf{h}}_k = \frac{1}{K}(\mathbf{h}_{d,k} + \sum_{i=1}^{N}\mathbf{h}_{0,i,k}\theta_i)^H(\hat{\mathbf{h}}_{d,k} + \sum_{j=1}^{N}\hat{\mathbf{h}}_{0,i,k}\theta_j), \tag{B.1}$$

$$\tag{B.2}$$

Noting the independence of $\hat{\mathbf{h}}_{d,k}$ and $\mathbf{h}_{0,i,k}$ vectors and applying **Lemma 3.2**.

$$\frac{1}{K}\mathbf{h}_k^H\hat{\mathbf{h}}_k - \frac{1}{K}\left(\mathbf{h}_{d,k}^H\hat{\mathbf{h}}_{d,k} + \mathbf{h}_{d,k}^H\sum_{j=1}^{N}\hat{\mathbf{h}}_{0,i,k}\theta_j + \sum_{j=1}^{N}\sum_{i=1}^{N}\theta_i^H\mathbf{h}_{0,i,k}^H\hat{\mathbf{h}}_{0,i,k}\theta_j\right) \xrightarrow[M,N,K\to\infty]{a.s.} 0, \tag{B.3}$$

Notice there are three separate terms in (B.3) so we find the deterministic equivalents for them separately.

Using (2.13), we obtain

$$\frac{1}{K}\mathbf{h}_{d,k}^H\hat{\mathbf{h}}_{d,k} = \frac{1}{K}\mathbf{h}_{d,k}^H(\mathbf{R}_{d,k}\mathbf{Q}_{d,k}(\mathbf{h}_{d,k} + \mathbf{n}_1^{UL})) \tag{B.4}$$

Next we notice the independence between $\mathbf{n}_1^{UL}$ and $\mathbf{h}_{d,k}^H$ and apply **Lemma 3.2** to obtain,

$$\frac{1}{K}\mathbf{h}_{d,k}^H\hat{\mathbf{h}}_{d,k} - \frac{1}{K}\mathbf{h}_{d,k}^H\mathbf{R}_{d,k}\mathbf{Q}_{d,k}\mathbf{h}_{d,k} \xrightarrow[M,N,K\to\infty]{a.s.} 0, \tag{B.5}$$

Given $\mathbf{h}_{d,k} \sim \mathcal{CN}(\mathbf{0}, \beta_{d,k}\mathbf{I}_M)$, we apply **Lemma 3.1** to obtain,

$$\frac{1}{K}\mathbf{h}_{d,k}^H\hat{\mathbf{h}}_{d,k} - \frac{1}{K}\beta_{d,k}tr(\mathbf{R}_{d,k}\mathbf{Q}_{d,k}) \xrightarrow[M,N,K\to\infty]{a.s.} 0. \tag{B.6}$$

We can simplify the expression by using the definitions of $\mathbf{R}_{d,k}$ and $\mathbf{Q}_{d,k}$ in (2.13) to obtain,

$$\frac{1}{K}\mathbf{h}_{d,k}^H\hat{\mathbf{h}}_{d,k} - \frac{1}{K}\frac{\beta_{d,k}^2 M}{\beta_{d,k} + \frac{1}{\rho_{tr}}} \xrightarrow[M,N,K\to\infty]{a.s.} 0 \tag{B.7}$$

Let's look at the second term in (B.3) and by applying (2.16).

$$\frac{1}{K}\mathbf{h}_{d,k}^H\sum_{j=1}^{N}\hat{\mathbf{h}}_{0,i,k}\theta_j = \frac{1}{K}\sum_{j=1}^{N}\mathbf{h}_{d,k}^H(\mathbf{R}_{0,i,k}\mathbf{Q}_{j,k}\tilde{\mathbf{r}}_{j,k}^{tr})\theta_j \tag{B.8}$$

$$= \frac{1}{K}\sum_{j=1}^{N}\mathbf{h}_{d,k}^H(\mathbf{R}_{0,j,k}\mathbf{Q}_{j,k}(\tilde{\mathbf{h}_{d,k}} + \mathbf{h}_{0,j,k} + \mathbf{n}_j^{UL}))\theta_j \tag{B.9}$$

We note that $\mathbf{h}_{d,k}^H$ is independent of $\mathbf{h}_{0,j,k}$ and $\mathbf{n}_j^{UL}$. Moreover, we recall that $\mathbf{h}_{d,k} = \tilde{\mathbf{h}}_{d,k} + \hat{\mathbf{h}}_{d,k}$ and notice that $\hat{\mathbf{h}}_{d,k}$ and $\tilde{\mathbf{h}}_{d,k}$ are independent. Under these observations, we apply **Lemma 3.2** successively to obtain

$$\frac{1}{K}\sum_{j=1}^{N}\mathbf{h}_{d,k}^H\hat{\mathbf{h}}_{0,j,k}\theta_j - \frac{1}{K}\sum_{j=1}^{N}\mathbf{h}_{d,k}^H\mathbf{R}_{0,j,k}\mathbf{Q}_{j,k}\tilde{\mathbf{h}}_{d,k}\theta_j \xrightarrow[M,N,K\to\infty]{a.s.} 0, \tag{B.10}$$

$$\frac{1}{K}\sum_{j=1}^{N}\mathbf{h}_{d,k}^H\mathbf{R}_{0,j,k}\mathbf{Q}_{j,k}\tilde{\mathbf{h}}_{d,k}\theta_j - \frac{1}{K}\sum_{j=1}^{N}\tilde{\mathbf{h}}_{d,k}^H\mathbf{R}_{0,j,k}\mathbf{Q}_{j,k}\tilde{\mathbf{h}}_{d,k}\theta_j \xrightarrow[M,N,K\to\infty]{a.s.} 0. \tag{B.11}$$

Next we apply the trace lemma on the quadratic term in $\tilde{\mathbf{h}}_{d,k}$ where $\tilde{\mathbf{h}}_{d,k} \sim \mathcal{CN}(\mathbf{0}, \mathbf{C}_{\tilde{\mathbf{h}}_{d,k}\tilde{\mathbf{h}}_{d,k}})$, where $\mathbf{C}_{\tilde{\mathbf{h}}_{d,k}\tilde{\mathbf{h}}_{d,k}}$ is defined in **Lemma 3.1**. The resulting convergence is given as

$$\frac{1}{K}\sum_{j=1}^{N}\mathbf{h}_{d,k}^H\hat{\mathbf{h}}_{0,j,k}\theta_j - \frac{1}{K}\sum_{j=1}^{N}tr(\mathbf{C}_{\tilde{\mathbf{h}}_{d,k}\tilde{\mathbf{h}}_{d,k}}\mathbf{R}_{0,j,k}\mathbf{Q}_{j,k})\theta_j \xrightarrow[M,N,K\to\infty]{a.s.} 0. \tag{B.12}$$

Next we look at the deterministic equivalence of third term by using the definitions in (2.15) and (2.16).

$$\frac{1}{K}\sum_{j=1}^{N}\sum_{i=1}^{N}\theta_i^*\mathbf{h}_{0,i,k}^H\hat{\mathbf{h}}_{0,j,k}\theta_j = \frac{1}{K}\sum_{j=1}^{N}\sum_{i=1}^{N}\theta_i^*\mathbf{h}_{0,i,k}^H(\mathbf{R}_{0,j,k}\mathbf{Q}_{j,k}\tilde{\mathbf{r}}_{j,k}^{tr})\theta_j \tag{B.13}$$

$$= \frac{1}{K}\sum_{j=1}^{N}\sum_{i=1}^{N}\theta_i^*\mathbf{h}_{0,i,k}^H(\mathbf{R}_{0,j,k}\mathbf{Q}_{j,k}(\tilde{\mathbf{h}}_{d,k}+\mathbf{h}_{0,j,k}+\frac{\mathbf{n}_j^{UL}}{\rho_{tr}}))\theta_j \tag{B.14}$$

Notice that $\mathbf{h}_{0,i,k}$ is independent of $\tilde{\mathbf{h}}_{d,k}$ and $\mathbf{n}_j^{UL}$ $\forall i, j$ and independent of $\mathbf{h}_{0,j,k}$ for $j \neq i$, and by applying **Lemma 3.2** we obtain:

$$= \frac{1}{K}\sum_{i=1}^{N}\theta_i^*\theta_i\mathbf{h}_{0,i,k}^H\mathbf{R}_{0,i,k}\mathbf{Q}_{i,k}\mathbf{h}_{0,i,k} \tag{B.15}$$

Now as $M, K \to \infty$ and by applying the trace lemma **Lemma 3.1** and noting that $\theta_i^*\theta_i = 1$

$$= \frac{1}{K}\sum_{i=1}^{N}\mathbf{h}_{0,i,k}^H\mathbf{R}_{0,i,k}\mathbf{Q}_{i,k}\mathbf{h}_{0,i,k} - \frac{1}{K}\sum_{i=1}^{N}tr(\mathbf{R}_{0,i,k}\mathbf{R}_{0,i,k}\mathbf{Q}_{i,k}) \xrightarrow[M,N,K\to\infty]{a.s.} 0 \tag{B.16}$$

Therefore, by (B.7), (B.12), and (B.16) we obtain:

$$\frac{1}{K}\mathbf{h}_k^H\hat{\mathbf{h}}_k - \frac{1}{K}\left(\frac{\beta_{d,k}^2 M}{\beta_{d,k}+\frac{1}{\rho_{tr}}} + \sum_{i=1}^{N}tr(\mathbf{C}_{\tilde{\mathbf{h}}_{d,k}\tilde{\mathbf{h}}_{d,k}}\mathbf{R}_{0,i,k}\mathbf{Q}_{i,k})\theta_i + \sum_{i=1}^{N}tr(\mathbf{R}_{0,i,k}\mathbf{R}_{0,i,k}\mathbf{Q}_{i,k})\right) \xrightarrow[M,N,K\to\infty]{a.s} 0. \tag{B.17}$$

Deterministic equivalent of $\frac{1}{K}\sum_{l\neq k}|\mathbf{h}_k^H\hat{\mathbf{h}}_l|^2 p_l$:

Note that $\frac{1}{K}\sum_{l\neq k}p_l|\mathbf{h}_k^H\hat{\mathbf{h}}_l|^2 = \frac{1}{K}\mathbf{h}_k^H\hat{\mathbf{H}}_{[k]}^H\mathbf{P}_{[k]}\hat{\mathbf{H}}_{[k]}\mathbf{h}_k$, where $\mathbf{H}_{[k]}$ $= [\mathbf{h}_1, \ldots, \mathbf{h}_{k-1}, \mathbf{h}_{k+1}, \ldots, \mathbf{h}_K]^H$. Also, note $\hat{\mathbf{H}}_{[k]}^H\mathbf{P}_{[k]}\hat{\mathbf{H}}_{[k]}$ is independent of $\mathbf{h}_k$. Moreover $\mathbf{h}_k$ defined in (2.5) is distributed as $\mathcal{CN} \sim (\mathbf{0}, \mathbf{A}_k)$ since $\mathbf{A}_k = \mathbb{E}[\mathbf{h}_k\mathbf{h}_k^H] = \mathbf{H}_1\mathbf{\Theta}\mathbb{E}[\mathbf{h}_{2,k}\mathbf{h}_{2,k}^H]\mathbf{\Theta}^H\mathbf{H}_1^H + \mathbb{E}[\mathbf{h}_{d,k}\mathbf{h}_{d,k}^H] = \beta_{2,k}\mathbf{H}_1\mathbf{H}_1^H + \beta_{d,k}\mathbf{I}_M$. Using these observations, as $M, K \to \infty$ and by applying **Lemma 3.1** we obtain:

$$\frac{1}{K}\mathbf{h}_k^H\hat{\mathbf{H}}_{[k]}^H\mathbf{P}_{[k]}\hat{\mathbf{H}}_{[k]}\mathbf{h}_k - \frac{1}{K}tr(\mathbf{A}_k\hat{\mathbf{H}}_{[k]}^H\mathbf{P}_{[k]}\hat{\mathbf{H}}_{[k]}) \xrightarrow[M,K\to\infty]{a.s} 0 \tag{B.18}$$

Notice $\frac{1}{K}tr(\mathbf{A}_k\hat{\mathbf{H}}_{[k]}^H\mathbf{P}_{[k]}\hat{\mathbf{H}}_{[k]}) = \frac{1}{K}\sum_{l\neq k} p_l\hat{\mathbf{h}}_l^H\mathbf{A}_k\hat{\mathbf{h}}_l$. Applying **Lemma 3.1** and as $M, K \to \infty$

$$\frac{1}{K}\sum_{l\neq k} p_l\hat{\mathbf{h}}_l^H\mathbf{A}_k\hat{\mathbf{h}}_l - \frac{1}{K}\sum_{l\neq k} p_l tr\mathbf{C}_l\mathbf{A}_k \xrightarrow[M,K\to\infty]{a.s} 0 \tag{B.19}$$

where $\mathbf{C}_k = E[\hat{\mathbf{h}}_k\hat{\mathbf{h}}_k^H]$ proven in Appendix A (D)

Therefore:

$$\frac{1}{K}\sum_{l\neq k} |\mathbf{h}_k^H\hat{\mathbf{h}}_l|^2 p_l - \frac{1}{K}\sum_{l\neq k} p_l tr\mathbf{C}_l\mathbf{A}_k \xrightarrow[M,K\to\infty]{a.s} 0 \tag{B.20}$$

Deterministic equivalent of $\frac{1}{K}\Psi = \frac{1}{K}tr(\mathbf{P}\hat{\mathbf{H}}\hat{\mathbf{H}}^H)$:

Note that,

$$\Psi = tr(\mathbf{P}\hat{\mathbf{H}}\hat{\mathbf{H}}^H) = \sum_{k=1}^{K} p_k\hat{\mathbf{h}}_k^H\hat{\mathbf{h}}_k \tag{B.21}$$

As $M, K \to \infty$ and by applying the **Lemma 3.1** on the quadratic form in $\hat{\mathbf{h}}_l$, we obtain

$$\frac{1}{K}\sum_{k=1}^{K} p_k\hat{\mathbf{h}}_k^H\hat{\mathbf{h}}_k - \frac{1}{K}\sum_{k=1}^{K} p_k tr\mathbf{C}_k \xrightarrow[M,K\to\infty]{a.s} 0 \tag{B.22}$$

Therefore:

$$\frac{1}{K}\Psi - \frac{1}{K}\sum_{k=1}^{K} p_k tr\mathbf{C}_k \xrightarrow[M,K\to\infty]{a.s} 0 \tag{B.23}$$

Combining (B.17), (B.20), and (B.23) we obtain the deterministic equivalent of SINR as shown in Theorem 3.1.

Appendix C

Proof of Corollary 3.4

The proof follows by writing $\gamma^{\circ}_{k,MRT}$ in Corollary 3.3 using the definition in (3.20) as,

$$\gamma^{\circ}_{k,MRT} = \frac{\frac{1}{K^2}|tr(\beta_{d,k}\mathbf{I}_M + c\beta_{d,k}\mathbf{D}\mathbf{D}^H)|^2}{\frac{1}{K^2}\sum_{l\neq k} tr((\beta_{d,k}\mathbf{I}_M + c\beta_{d,k}\mathbf{D}\mathbf{D}^H)^2) + \frac{\frac{1}{K^2}\sum_{l=1}^{K} tr(\beta_{d,l}\mathbf{I}_M + c\beta_{d,l}\mathbf{D}\mathbf{D}^H)}{\rho}}, \tag{C.1}$$

$$= \frac{\beta^2_{d,k}(cMN + M)^2}{\sum_{l\neq k}\beta_{d,l}\beta_{d,k}(c^2MN^2 + 2cMN + M) + \frac{\sum_{l=1}^{K}\beta_{d,l}(cMN+M)}{\rho}}, \tag{C.2}$$

$$= \frac{\beta_{d,k}(cMN + M)}{\sum_{l\neq k}\beta_{d,l}M\frac{(cN+1)^2}{M(cN+1)} + \frac{\sum_{l=1}^{K}\beta_{d,l}}{\beta_{d,k}\rho}}, \tag{C.3}$$

$$= \frac{\beta_{d,k}(cMN + M)}{\sum_{l\neq k}\beta_{d,l}(cN + 1) + \frac{\sum_{l=1}^{K}\beta_{d,l}}{\beta_{d,k}\rho}}, \tag{C.4}$$

$$= \frac{1}{\frac{1}{M}\sum_{l\neq k}\frac{\beta_{d,l}}{\beta_{d,k}} + \frac{\sum_{l=1}^{K}\beta_{d,l}}{M\beta^2_{d,k}\rho(cN+1)}}, \tag{C.5}$$

where (C.2) is obtained by noting that $tr(\beta_{d,k}\mathbf{I}_M + c\beta_{d,k}\mathbf{D}\mathbf{D}^H) = \beta_{d,k}(M + cMN)$ and $tr(\mathbf{D}\mathbf{D}^H\mathbf{D}\mathbf{D}^H) = MN^2$. This completes the proof of Corollary (3.4).

Appendix D

Proof of Lemma 3.4

In this section, we derive the derivative expression in **Lemma 3.4**. To begin, we can look at the deterministic equivalent defined in (3.8) and use the linearity property of the derivative to find the derivative of the expression:

$$\frac{\partial R^o_{sum}}{\partial \theta_i} = \sum_{k=1}^{K} \frac{\partial \log(1+\gamma^o_k)}{\partial \theta_i} \tag{D.1}$$

$$= \sum_{k=1}^{K} \frac{1}{(1+\gamma^o_k)\ln(2)} \frac{\partial(\gamma^o_k)}{\partial \theta_i} \tag{D.2}$$

Now we can look at the deterministic equivalent γ^o_k defined in (3.6) and notice that it is a quotient of two terms, i.e. the numerator $\frac{p_k}{K}|n_k|^2$ and the denominator $d = \sum_{l \neq k} \frac{p_l}{K} tr(\mathbf{C}_l \mathbf{A}_k) + \frac{\frac{p_k}{K}\sum_{k=1}^{K} tr\mathbf{C}_k}{\rho}$. Following the quotient rule ,the derivative of the deterministic equivalence of SINR at user k with respect to θ_i can then be defined as:

$$\frac{\partial \gamma^o_k}{\partial \theta_i} = \frac{\frac{p_k}{K}\frac{\partial |n_k|^2}{\partial \theta_i}(d) + \frac{p_k}{K}|n_k|^2 \frac{\partial d}{\partial \theta_i}}{d^2} \tag{D.3}$$

where the gradient can be expressed as: $\nabla \gamma^o_k = [\frac{\partial \gamma^o_k}{\partial \theta_1}, \frac{\partial \gamma^o_k}{\partial \theta_2} \ldots \frac{\partial \gamma^o_k}{\partial \theta_N}]$

In the following two subsection, we will derive the expression for the following terms: $\frac{\partial |n_k|^2}{\partial \theta_i}$ and $\frac{\partial d}{\partial \theta_i}$, separately.

D.1 Proof of Derivative Expression for $\frac{\partial n_k}{\partial \theta_n}$

Notice that $|n_k|^2$ is nothing but the norm squared, in which we may use the power rule to find the derivative as follows: $\frac{\partial |n_k|^2}{\partial \theta_i} = \frac{2p_k}{K}|n_k|\frac{\partial n_k}{\theta_i}$

Recall:
$n_k = \sum_{i=1}^{N} v_i tr(\mathbf{C}_{\tilde{\mathbf{h}}_{d,k}\tilde{\mathbf{h}}_{d,k}}\mathbf{R}_{0,i,k}\mathbf{Q}_{i,k}) + \frac{\beta_{d,k}^2 M}{\beta_{d,k}+\frac{1}{\rho_{tr}}} + \sum_{i=1}^{N} tr(\mathbf{R}_{0,i,k}\mathbf{R}_{0,i,k}\mathbf{Q}_{i,k})$

Notice that only the first term $\sum_{i=1}^{N} \theta_i tr(\mathbf{C}_{\tilde{\mathbf{h}}_{d,k}\tilde{\mathbf{h}}_{d,k}}\mathbf{R}_{0,i,k}\mathbf{Q}_{i,k})$ includes the θ_i term. For this reason, it can be easily shown that:
$\frac{\partial n_k}{\partial \theta_i} = tr(\mathbf{C}_{\tilde{\mathbf{h}}_{d,k}\tilde{\mathbf{h}}_{d,k}}\mathbf{R}_{0,i,k}\mathbf{Q}_{i,k})$. Therefore:

$$\frac{\partial |n_k|^2}{\partial \theta_i} = \frac{2p_k}{K}|n_k| tr(\mathbf{C}_{\tilde{\mathbf{h}}_{d,k}\tilde{\mathbf{h}}_{d,k}}\mathbf{R}_{0,i,k}\mathbf{Q}_{i,k}) \tag{D.4}$$

D.2 Proof of (3.26)

We will now derive the derivative $d' = \frac{\partial d_k}{\partial \theta_n}$ of the denominator $d_k = \sum_{l\neq k} \frac{p_l}{K} tr(\mathbf{C}_l\mathbf{A}_k) + \frac{\frac{p_k}{K}\sum_{k=1}^{K} tr\mathbf{C}_k}{\rho}$ as,

$$\frac{\partial d}{\partial \theta_n} = \sum_{l\neq k} \frac{p_l}{K} tr\left(\frac{\partial \mathbf{C}_l\mathbf{A}_k}{\partial \theta_n}\right) + \frac{p_k}{K\rho}\sum_{k=1}^{K} tr\left(\frac{\partial \mathbf{C}_k}{\partial \theta_n}\right), \tag{D.5}$$

where $\mathbf{C}_l = \frac{\beta_{d,l}^2}{\beta_{d,l}+\frac{1}{\rho_{tr}}} + \sum_{i=1}^{N} \mathbf{R}_{0,i,l}\mathbf{Q}_{i,l}(\mathbf{R}_{0,i,l} + \frac{\mathbf{I}_M}{\rho_{tr}})\mathbf{Q}_{i,l}^H\mathbf{R}_{0,i,l}^H$

$$+ \sum_{j=1}^{N}\sum_{i=1}^{N} \theta_i \mathbf{R}_{0,i,l}\mathbf{Q}_{i,l}\mathbf{C}_{\tilde{\mathbf{h}}_{d,l}\tilde{\mathbf{h}}_{d,l}}\mathbf{Q}_{j,l}^H\mathbf{R}_{0,j,l}^H\theta_j^*.$$

Noting that $tr(\mathbf{C}_l\mathbf{A}_k)$ and $tr(\mathbf{C}_k)$ are real valued functions of the complex variable θ_n, for which we have the expression

$$\frac{\partial tr(\mathbf{C}_l\mathbf{A}_k)}{\partial \theta_n} = 2\frac{\partial tr(\mathbf{C}_l\mathbf{A}_k)}{\partial \theta_n^*}, \tag{D.6}$$

$$\frac{\partial tr(\mathbf{C}_k)}{\partial \theta_n} = 2\frac{\partial tr(\mathbf{C}_k)}{\partial \theta_n^*}. \tag{D.7}$$

Only the third term in the expression of $\mathbf{C}_l$ given as

$\sum_{j=1}^{N}\sum_{i=1}^{N}\theta_i\mathbf{R}_{0,i,l}\mathbf{Q}_{i,l}\mathbf{C}_{\tilde{\mathbf{h}}_{d,l}\tilde{\mathbf{h}}_{d,l}}\mathbf{Q}_{j,l}^{H}\mathbf{R}_{0,j,l}^{H}\theta_j^*$ will contribute to the derivative. Using this we can obtain

$$\frac{\partial tr(\mathbf{C}_l\mathbf{A}_k)}{\partial\theta_n^*} = \sum_{i=1}^{N}\theta_i tr(\mathbf{R}_{0,i,l}\mathbf{Q}_{i,l}\mathbf{C}_{\tilde{\mathbf{h}}_{d,l}\tilde{\mathbf{h}}_{d,l}}\mathbf{Q}_{n,l}^{H}\mathbf{R}_{0,n,l}^{H}\mathbf{A}_k), \tag{D.8}$$

$$\frac{\partial tr(\mathbf{C}_k)}{\partial\theta_n^*} = \sum_{i=1}^{N}\theta_i tr(\mathbf{R}_{0,i,k}\mathbf{Q}_{i,k}\mathbf{C}_{\tilde{\mathbf{h}}_{d,k}\tilde{\mathbf{h}}_{d,k}}\mathbf{Q}_{n,k}^{H}\mathbf{R}_{0,n,k}^{H}). \tag{D.9}$$

Plugging (D.8) and (D.9) in (D.6) and (D.7) respectively and using the resulting expressions in (D.5), we obtain $\frac{\partial d}{\partial\theta_n}$. Plugging (D.5) and (D.4) in (D.3) will complete the proof of Lemma 3.4.